DEVELOPMENT OF TRACER RELATIONS AND CHEMICAL OZONE LOSS DURING THE SETUP PHASE OF THE POLAR VORTEX

Simone Tilmes[1,3], Rolf Müller[1], Jens-Uwe Grooß[1], Hideaki Nakajima[2] and Yasuhiro Sasano[2]

[1]Institute of Stratospheric Research (ICG-I), Research Centre Jülich, Jülich, Germany

[2]Atmospheric Environment Division, National Institute for Environmental Studies, Japan

[3]currently at National Center for Atmospheric Research, Boulder, CO, USA

Short title: OZONE LOSS DURING THE SETUP OF THE POLAR VORTEX.

Abstract. The development of tracer-tracer relations n the polar stratosphere is analyzed during the time when the vortex forms and a westerly circulation develops after polar summer (the setup phase of the polar vortex). We consider high southern latitudes from March to June for the winters 1997 and 2003 and high northern latitudes from September to October 2003. ILAS and ILAS-II satellite observations and model simulations are used to investigate chemical changes in O_3, NO_2 and HNO_3 during these periods. Tracer-tracer relations and meteorological analyses consistently indicate a separation of the incipient polar vortex into two parts. The area within the edge of the inner vortex is isolated from the outer part that is still influenced by mixing with air of mid-latitude origin. In the Antarctic in April, ozone concentrations vary by about 0.5 ppmv within the isolated inner vortex between 500 and 600 K potential temperature. This inhomogeneous distribution of ozone is likewise obvious in MIPAS satellite measurements. Box model simulations explain the low ozone concentrations in April caused by chemical ozone loss due to catalytic cycles that are mainly driven by NO_x at this time of the year. The simulations also explain the observed conversion of NO_x to HNO_3 during the setup phase of the 2003 Antarctic vortex. During June in the Antarctic, the internal vortex transport barrier disappears and ozone mixing ratios become homogeneous throughout the entire vortex. At that time, no further ozone loss occurs because of the lack of sunlight.

1. Introduction

During the past decade much research was devoted to chemical ozone loss in the Arctic winter lower stratosphere (LS). Ozone mixing ratios in the polar winter are controlled by both dynamical and chemical processes in the polar vortex. The descent of air in the polar region of both the Arctic and Antarctic vortex [e.g., *Russell et al.*, 1993; *Rosenfield et al.*, 1994], which is most effective at the beginning of the winter [e.g., *Müller et al.*, 1996; *Kawamoto et al.*, 2004; *Konopka et al.*, 2004], increases ozone mixing ratios at a given altitude in the LS during winter and spring. According to current understanding, polar ozone loss in the LS occurs in winter and spring within the polar vortex and is mainly due to ClO_x and BrO_x chemistry, starting with the illumination of the polar region after the darkness of winter [e.g., *Solomon*, 1999]. Owing to the existence of polar stratospheric clouds (PSCs), chlorine is activated from its reservoirs. Effective catalytic cycles driven by active chlorine and bromine destroy ozone. In spring, the polar vortex weakens, becomes distorted, and finally breaks down. A rapid easterly acceleration occurs in conjunction with warming of polar air resulting in the formation of the summertime anticyclone. During polar summer, ozone is destroyed by NO_x-catalyzed cycles [e.g., *Farman*, 1985; *Brühl et al.*, 1998; *Fahey and Ravishankara*, 1999; *Crutzen and Brühl*, 2001]. Therefore, ozone mixing ratios decrease in the LS until the polar vortex starts to form again in fall.

At present, few observations are available to investigate the dynamical and chemical processes controlling ozone and other tracers during the formation of the polar vortices. *Kawa et al.* [2002] analyzed the evolution of ozone during the setup phase of the northern hemisphere (NH) polar vortex in fall 1999, using in-situ data from the Observations of the Middle Stratosphere (OMS) balloon platform, satellite data from the Polar Ozone and Aerosol Measurement III (POAM III) instrument and a chemistry and transport model (CTM). In the study by *Kawa et al.* [2002] it is shown that in late summer a minimum in ozone and its variance in high northern latitudes are the result of two processes. First, with increasing

wave-driven transport in fall ozone-rich air is transported from lower latitudes polewards whereas ozone-poor air is located close to the pole [*Brühl et al.*, 1998; *Kawa et al.*, 2002]. Second, net photochemical loss accelerated with decreasing solar illumination because the shorter wavelength necessary for ozone production are absorbed more strongly at low solar elevations in autumn whereas ozone loss from radical catalytic cycles is still effective [*Perliski et al.*, 1989; *Farman et al.*, 1985]. Therefore, enhanced chemical ozone destruction occurs during this time of the year. In the study by *Kawa et al.* [2002], only one particular Arctic fall was investigated.

In the present study, the formation process of the vortex is discussed for two Antarctic and one Arctic winter using analyses from the UK Meteorological Office (MetO) [*Swinbank and O'Neill*, 1994]. The existence of a polar vortex edge is defined by the existence of a maximum vorticity gradient (∇PV) constrained by the wind velocity (v) with regard to equivalent latitudes, as proposed by *Nash et al.* [1996]. Here, the value of the maximum vorticity gradient times wind velocity ($\nabla PV \cdot v$) is employed to identify an additional transport barrier located within the vortex edge. Measurements of ILAS (Improved Limb Atmospheric Spectrometer) aboard ADEOS (Advanced Earth Observing Satellite) and ILAS-II aboard ADEOS-II show a separation of air masses located in the different regions of the vortex using the tracer-tracer correlation method, a method to separate chemical ozone loss from dynamical processes [e.g., *Proffitt et al.*, 1993; *Tilmes et al.*, 2003, 2004; *Müller et al.*, 2005]. A study by *Lee et al.* [2001] found two distinct regions of the Antarctic vortex between July and the end of October, based on model simulations, where the inner vortex remains isolated between late winter and spring. Here, we show that the inner vortex is only intermittently present during May and June in winters 2003 and 1997 and during the entire Antarctic winter 2003 [*Tilmes et al.*, 2006b].

To identify chemical changes and calculate chemical ozone loss during winter and spring using tracer-tracer correlations, an early winter reference function is

derived to describe the chemically undisturbed conditions inside a sufficiently isolated early vortex [e.g., *Müller et al.*, 2002; *Tilmes et al.*, 2003, 2004; *Müller et al.*, 2005]. A threshold value used to define a sufficiently impermeable vortex is given below. The development of the early Arctic vortex 1996–97 from November to January was earlier analyzed by *Tilmes et al.* [2003] based on Version 6 ILAS observations. In that study, it was shown that it is important to carefully determine the time in winter when ozone mixing ratios are homogeneous at a certain N_2O level to determine a valid early winter reference function. This is the time when the vortex is isolated and compact O_3/N_2O correlations are established. In a very weak early vortex mixing across the vortex edge may change tracer-tracer correlation in such a way that larger ozone mixing ratios may result and chemical ozone loss may therefore be underestimated. *Müller et al.* [2005] discussed the influence of mixing processes on tracer-tracer correlations in the polar region in detail and showed that mixing processes cannot change the deduced chemical ozone loss significantly in an isolated polar vortex. Here, it will be shown that tracer-tracer correlations within the vortex of the southern hemisphere (SH) in June 2003 describe a compact relationship at a time when the transport barrier at the edge of the vortex is established.

In this paper, ILAS and ILAS-II observations will be described in Section 2. The setup phase of the 2003 Antarctic vortex will be investigated in Section 3 based on the analysis of MetO data and on ILAS-II observations. Further, a comparison with simulations of the Chemical Lagrangian Model of the Stratosphere (CLaMS) box model [*McKenna et al.*, 2002b, a] and with the Michelson Interferometer for Passive Atmospheric sounding (MIPAS) observations [e.g., *Fischer and Oelhaf*, 1996] is performed for the 2003 Antarctic winter. We utilize the ESA MIPAS reprocessed Level 2 data set with Instrument Processing Facility version 4.61. In Section 4, the setup phase of the 1997 Antarctic vortex is described based on meteorological analyses and ILAS observations and a comparison between the two Antarctic winters 2003 and 1997 is made. The additional use of ILAS-II

observations in September and October 2003 and ILAS Version 6 observations will allow further insights into the setup phase of the Arctic vortex as described in Section 4. Finally, conclusions are given in Section 5.

2. Measurements by ILAS and ILAS-II

Measurements by the two instruments ILAS (Improved Limb Atmospheric Spectrometer) aboard ADEOS and ILAS-II aboard ADEOS-II were used in this study. These two instruments measured atmospheric trace gases using the solar occultation technique at high latitudes in both hemispheres (between 54°N and 71°N and 64°S to 88°S). Observations of the altitude distribution of ozone, HNO_3, N_2O, CH_4, and of the aerosol extinction coefficient at 780 nm data from cloud top up to 70 km are available. Vertical profiles of other atmospheric trace gases, measured by ILAS-II, such as NO_2, H_2O, $ClONO_2$, and N_2O_5, are also retrieved during the entire measurement period but have not been validated yet and will not be used in this study. The accuracy of the ozone is estimated to be better than ±10% [*Sugita et al.*, 2006].

ILAS performed observations for eight months between October 1996 and June 1997. These measurements cover the entire Arctic winter 1996–97 [*Suzuki et al.*, 1995; *Sasano et al.*, 1999]. ESA MIPAS reprocessed Level 2 data set with ¿ Instrument Processing Facility version 4.61 ILAS-II observations covered the period from March to October 2003, during an entire Antarctic winter period and the setup phase of the 2003 Arctic vortex [*Nakajima et al.*, 2005]. To investigate the development of the Antarctic polar vortex in 1997 and in 2003, March to June observations of both data sets are used.

ILAS-II Version 1.4 and ILAS Version 6.0 ozone, N_2O, HNO_3, and NO_2 (only from ILAS [*Yokota et al.*, 2005]) are used in this study. Applying the tracer-tracer correlation method, N_2O is used as a long-lived tracer for both the ILAS and ILAS-II analysis. For ILAS, the uncertainty for N_2O data is better than 10% over 10-30 km which is of sufficient quality to be used here [*Kanzawa et al.*, 2003]. For

ILAS-II, N_2O is up to 20% too low for mixing ratios less than 100 ppbv during March to June 2003 in the SH compared to measurements of the Sub-Millimeter Radiomenter (SMR) (v1.2) aboard the Swedish mini-satellite ODIN [*Ejiri et al.*, 2006]. This is also the case during September and October 2003 in the NH. However, no significant seasonal change in this low bias is found. Thus, although N_2O likely has an instrumental offset compared to SMR measurements (which depends on altitude), since the offset does not vary seasonally, it will not affect the results of tracer-tracer correlations.

3. The setup phase of the Antarctic vortex 2003

Tracer-tracer correlations are used to investigate the development of ozone, HNO_3 and NO_2 inside the incipient polar vortex [1]. This section presents results from March to June 2003 for the Antarctic.

The edge of the polar vortex is determined here according to the definition of *Nash et al.* [1996], whereby the edge is defined as being co-located with the maximum potential vorticity gradient (∇PV) that is closest to the polar night jet. *Nash et al.* [1996] used 15.2 m/s as an empirically determined limit below which a vortex edge can not be defined. As soon as a vortex edge can be identified in fall according to this definition, we assume that a vortex has started to form. At first, the equivalent latitude filter of the *Nash et al.* [1996] algorithm was used to filter transport barriers between 45 and 80 degrees. In this way, the detected vortex edged switched between two transport barrier that are about equally strong (not shown). Therefore, to identify both the two potential transport barriers at the same time, we applied this equivalent latitude filter twice, for the interval

[1]Here, the setup phase of the vortex, the period September/November for the Arctic [*Kawa et al.*, 2002], and March/May for the Antarctic, is referred to as the "incipient" vortex. Earlier, the phase of the developing vortex in March/April in the Antarctic and in November in the Arctic has been referred to as *proto-vortex* [e.g., *Michelsen et al.*, 1998]."

between 40 degrees and 70 degrees and for the interval poleward of 70 degrees. The threshold value of 70°S is empirically determined considering the pattern of $\nabla PV \cdot v$ with regard to equivalent latitudes and time (as described below, see Figure 1). We define the edge derived poleward of 70°S as the 'inner vortex edge' and the area inside as the 'inner vortex'. Further, the edge derived equatorward of 70°S is defined as the 'outer vortex edge' and the area inside is referred to as the 'outer vortex'. In the case two vortex edges are present at the same time, the region within the poleward edge of the outer/inner vortex is referred to as 'outer/inner vortex core'. If only one vortex edge exists the enclosed area is referred to as the 'entire vortex' as shown in Figure 2. (One edge at exactly 70°S will also be referred to as the entire vortex edge).

Figure 1.

Figure 2.

The potential vorticity gradient, ∇PV (solid line), the wind velocity (dotted line) and the value $\nabla PV \cdot v$ (dashed line) are shown in Figure 2. A wind jet is co-located with both the inner and outer maximum PV gradient that suggest the existence of a double edge structure of the vortex during this time of the year.

In Figure 1 $\nabla PV \cdot v$ is shown as a function of time over the setup phase of the vortex at 475, 550, and 650 K for the Antarctic winter 2003. Here and in the following the modified PV [*Lait*, 1994] is used to allow the comparison of $\nabla PV \cdot v$ at different altitudes. White crosses show the location of the vortex edge according to the definition by *Nash et al.* [1996]. However, the existence of a vortex edge derived with this criterium is not sufficient to assume an impermeable polar vortex edge. *Steinhorst et al.* [2005] performed a CLaMS model study to estimate a threshold value of the maximum PV gradient (∇PV), which characterizes a 'sufficiently impermeable' vortex edge for the Arctic winter 1999-2000. Using the modified potential vorticity [*Lait*, 1994] this threshold value was found to be 1.5 PVU/degree. Further *Steinhorst et al.* [2005] have shown that if the maximum ∇PV is less than this threshold value, mixing might occur locally in some segments with weak PV gradients, but it is not found that mixing into the vortex occurs across the whole contour. Here, we assume that the polar vortex is isolated if the

maximum of modified PV gradient times wind velocity exceeds a threshold value of 22.8 PVU/degree · m/s, derived using the threshold value 1.5 PVU/degree [*Steinhorst et al.*, 2005] times 15.2 m/s [*Nash et al.*, 1996].

The polar vortex started developing at the beginning of March 200 at altitudes above 475 K potential temperature. In the first half of March, one vortex edge exists at 70°S equivalent latitude (see Figure 1, white plus signs, top and middle panel), however the maximum $\nabla PV \cdot v$ is far below the threshold value for an isolated vortex. Therefore, the degree of isolation of the vortex is expected to be small. During the second half of March and the first half of April $\nabla PV \cdot v$ shows two relative maxima that exist almost continuously poleward of 50°S at 650 K. Correspondingly, an inner and outer vortex edge exists (see Figure 1, top panel). At the end of March, the polar vortex consists of two parts that are separated, because each of the maxima exceeds the threshold value for an isolated vortex (defined above) and might constitute a transport barrier. At 550 K, during the first half of April, the inner vortex edge exists almost continuously whereas an isolated outer vortex does not exist continuously before mid-April 2003 (see Figure 1, middle panel).

Figure 3.

The described synoptic situation is illustrated for three days in Figure 3. The PV distribution at two different potential temperature levels (650 K and 550 K) indicates that the vortex consists of two isolated regions. Further, the different characteristic of the two air masses, that is lower ozone mixing ratios within the inner vortex and larger ozone mixing ratios outside the inner vortex edge is clearly obvious at the beginning of April (as described in the following).

Figure 4.

Indeed, in Figure 3 back trajectory calculations show that air masses observed by ILAS-II poleward of 75°S equivalent latitude stay within the area of the inner vortex between March 10 and April 2-4, 2003, at altitudes above the 150 ppbv N_2O level; ≈ at 500 K potential temperature during this time of the year (see Figure 5, top panel). Therefore, the inner vortex is well isolated from the outer vortex during this period. At altitudes below 500 K, air masses arrive on average from

Figure 5.

equivalent latitudes equatorward of 75°S. This is in agreement with the fact that no vortex edge was calculated at 475 K so that the polar area is less isolated at these altitudes.

An outer vortex edge has existed continuously since the end of March at 650 K and since mid-April at 475 and 550 K. The entire vortex can now be expected to be isolated from air outside the vortex, because the local maximum $\nabla PV \cdot v$ clearly exceeds the threshold value (defined above); a behavior also shown by numerous earlier studies [e.g., *Juckes and McIntyre*, 1987; *Pierce and Fairlie*, 1993; *Manney et al.*, 1994]. In Section 3.1, the tracer development during the setup phase of the vortex will be discussed within this meteorological context.

Figure 6.

In Figure 6, the averaged solar illumination in sunlit hours per day is shown at 550 K for different equivalent latitudes between 55°S and 90°S. Average values of sunlit hours for different time intervals and equivalent latitudes are summarized in Table 1. In early March, the area within equivalent latitudes poleward of 55°S is strongly illuminated with more than 12 sunlit hours per day. In the second half of March and the first half of April, solar illumination decreases depending on equivalent latitude. From the second part of April, the vortex is hardly illuminated by the sun anymore at 80°S. After May 2003, the entire area poleward of 80°S is in darkness. Interestingly, the inner vortex edge seems to disappear at the time when the polar night reaches the location of the inner vortex edge.

Table 1.

Figure 7.

At the beginning of the Antarctic winter in March, MIPAS observations that are taken over the entire polar region of the SH show very inhomogeneous ozone concentrations in the just established and weak inner vortex at 650 K potential temperature (see Figure 7, first panel). Further, ozone-rich air is transported to the polar region by the Brewer-Dobson circulation and increases the ozone mixing ratios in the polar region. During the second half of March and April, patches of air with low ozone mixing ratios mix with those with greater ozone mixing ratios within the inner vortex (see Figure 7, second panel). During April, an inner and an outer transport barrier seems to exists, although partly intermittent as derived

using the *Nash et al.* [1996] criterion (see Figure 1, top panel). In May, although the inner vortex edge does not exists any more, air masses with smaller ozone mixing ratios are still close to the pole surrounded by air with greater ozone mixing ratios. Air masses slowly mix and homogenize within the established entire vortex. During June, ozone mixing ratios in the entire vortex are almost homogeneous distributed, only a few patches of air with low ozone mixing ratios still exist, as shown in Figure 7, bottom panel.

During the development of the vortex, both changing transport conditions (described above) and changing chemical processes – because the solar radiation that reaches the area around the south pole is decreasing – influence the mixing ratios of chemical constituents. A detailed description of these processes follows.

3.1. O_3/N_2O Development during the setup phase of the Antarctic vortex 2003

Figure 8.

Figure 9.

O_3/N_2O profiles measured inside the inner vortex core and inside the core of the entire vortex between 475 and 650 K from March to June 2003 are investigated in Figure 8. Additionally, ozone at different equivalent latitude regions for two specific N_2O levels with is shown as a time series between March 19 and May 22 to visualize the temporal development of ozone mixing ratios in dependence to equivalent latitudes (see Figure 9).

The first ILAS-II observations inside the developing Antarctic vortex were obtained from March 19 and 22, 2003 (see Figure 8). During this period, no inner polar vortex exists below 550 K. The O_3/N_2O relationship for the profiles measured in the core of the entire vortex can be described by an empirically derived reference function that is established for the time prior to polar night (see Figure 8, panel a, black line). Using N_2O as a long-lived tracer (mixing ratios in ppbv) and ozone (mixing ratios in ppmv) this incipient vortex reference function (valid for 30 ppbv $< N_2O <$ 300 ppbv) is:

$$O_3 = 3.03 \cdot 10^{-9} \cdot (N_2O)^4 - 1.93 \cdot 10^{-6} \cdot (N_2O)^3 + 3.78 \cdot 10^{-4} \cdot (N_2O)^2 \quad (1)$$

$$-3.07 \cdot 10^{-2} \cdot (\mathrm{N_2O}) + 3.38$$

The standard deviation of the O_3/N_2O relationship is $\sigma = 0.18$ ppmv, which will be defined as the range of uncertainty of the reference function. Between April 1 to 14, 2003, an inner vortex edge is observed above 475 K and additionally, an outer vortex edge exists above 550 K, as shown in Figure 1. ILAS-II profiles are available in both of these vortex regions. A separation between profiles inside the inner vortex region (Figure 8, green profiles, panel b) and inside the outer vortex is clearly observed for $N_2O < 150$ ppbv (Figure 8, panel b) and above 500 K in Figure 5 (bottom panel). N_2O profiles show the lowest mixing ratios at a given potential temperature level for profiles measured within the inner vortex core, which means the vortex air masses descended most strongly at the highest latitudes.

Profiles inside the inner vortex region and poleward of 80°S in early April scatter below the incipient vortex reference function estimated from March profiles (see Figure 8, panel b) by up to 0.5 ppmv ozone mixing ratios especially at the 100 ppmv N_2O level (550 K, see Figure 5, bottom panel). Figure 9 shows low ozone mixing ratios poleward of 77.5°S equivalent latitude with a variability of more than 0.5 ppmv during the first part of April 2003. Although the inner polar vortex is isolated (as shown above), ozone in the inner vortex region is not homogeneously distributed during the development of the polar vortex, as shown in Figure 7. Further, the measurements that are located equatorward of the inner vortex edge and 77.5°S (Figure 9) are characterized by significantly greater ozone mixing ratios (up to ≈ 1 ppmv) compared to values described by the incipient vortex reference function. These values also show a variability of more than 0.5 ppmv around their average values. These observations are consistent with the interpretation that the outer region of the entire vortex is influenced by mixing-in of ozone-rich air from outside the vortex, because no outer vortex edge was observed at the beginning of April below 650 K (see Figure 1).

During the first part of April, several ILAS-II ozone measurements show

mixing ratios that are significantly smaller than the values describing the incipient vortex reference function. Patches of very low ozone concentrations exist at lower latitudes that are not sampled by ILAS-II in March, as shown in Figure 7, top right panel. However, during April, some of the ILAS-II observations are located within the very low ozone patches (see Figure 7, bottom panel). Therefore, the significantly smaller ozone mixing ratios in early April visible in both the O_3/N_2O scatter plots and the potential temperature profiles may be a result of a different sampling of the ILAS-II instrument in late March and early April. On the other hand, a reduction of ozone in the isolated inner vortex can be caused by chemical ozone loss [*Kawa et al.*, 2002], see Section 3.3.

In a similar manner to the deduction of chemical ozone loss in late winter and early spring [e.g., *Tilmes et al.*, 2004], the tracer-tracer correlation method can be employed to derive chemical ozone loss in the isolated inner vortex in April 2003 using ILAS-II observations. For this purpose, we include the possible effect of a different sampling in the analysis. It has to be kept in mind that the influence of possibly occurring isentropic mixing across the inner transport barrier of the vortex might result in increasing ozone mixing ratios. This was shown for the polar vortex in late winter by *Müller et al.* [2005]. The amount of chemical ozone depletion that occurs at this time of the year will be further investigated using CLaMS box model simulations (see Section 3.3).

During April 15–30, the separation between ozone concentrations at different equivalent latitudes is more pronounced (Figure 8, panel c, and Figure 9). The profiles located inside the inner vortex core (Figure 8, panel c, green symbols) still show the lowest ozone mixing ratios with a slight increase compared to early April at altitudes corresponding to $N_2O \approx 100$ ppbv (500 K, see Figure 5). The entire polar vortex is isolated from the surrounding mid-latitude air, as described above, and, correspondingly, ozone mixing ratios of the entire vortex do not further increase. For the inner vortex, no further decrease of ozone mixing ratios that is no further chemical ozone depletion is detected in accordance with the lack of

insolation (see Figure 6).

Between the end of April and the beginning of May, ozone-tracer relations indicate a decrease of ozone measured at equivalent latitudes between 70°Sand 75°S, Figure 8, panels c and d, blue diamonds, and Figure 9. Likewise, during May and the beginning of June, ozone mixing ratios slightly decrease between 60°Sand 70°S for N_2O values smaller 150 ppbv, panels d to f, red diamonds. Thus, the effect of ozone depletion owing to decreasing solar radiation is observed at all equivalent latitudes sampled by ILAS-II. Further, at the end of May 2003, observations made outside the vortex display completely different ozone-tracer relations characterized by greater ozone mixing ratios (not shown). Thus, the entire vortex is isolated at this time of the year. By June, insolation goes to zero for all equivalent latitudes in the entire vortex and ozone mixing ratios become slowly uniform due to mixing within the vortex. Still in early June, the lowest ozone mixing ratios are measured at the equivalent latitudes furthest poleward (Figure 8, cyan and blue profiles in panel f). However, the very low ozone mixing ratios of ≈ 2 ppmv and less for N_2O < 150 ppbv observed during the first two weeks of April have vanished.

A new compact O_3/N_2O relationship has developed by mid-June when the vortex is well isolated and ozone in the entire vortex has become uniform. This new relationship, characterized by larger ozone mixing ratios compared to the incipient relationship, is used as an early winter reference function to derive chemical ozone depletion in late winter and spring, after the polar night as in *Tilmes et al.* [2006b].

3.2. HNO_3/N_2O Development during the setup phase of the Antarctic vortex 2003

During the setup phase of the 2003 Antarctic vortex, any observed ozone depletion cannot be a result of chemistry due to activated halogen compounds, because no supercooled ternary solution particles (STS) or polar stratospheric clouds (PSCs) were observed by the MIPAS before mid-May [*Spang et al.*, 2005]. Below 40 km, the most important ozone loss cycle involves NO_x radicals [*Crutzen*,

1970]:

$$\begin{aligned} NO_2 + O &\longrightarrow NO + O_2 \\ NO + O_3 &\longrightarrow NO_2 + O_2 \\ - - - & \\ \text{Net}: \quad O + O_3 &\longrightarrow 2O_2 \end{aligned} \tag{2}$$

With decreasing illumination between March and April, a larger amount of nitrogen is contained in longer-lived odd-nitrogen reservoir gases and therefore NO_x decreases. Besides N_2O_5, the major nitrogen reservoir is HNO_3. During the polar night NO_2 is very low. However, during April, enough sunlight – 4.2 sunlit hours per day at 70°S (see Table 1) – is still present and NO_2 and N_2O_5 are photolyzed rapidly so that a chemical equilibrium between NO_2 and NO develops. Thus, ozone can be chemically destroyed by the NO_x-catalyzed cycles (Eq. 2).

Figure 10.

As for O_3/N_2O, an empirical relationship of HNO_3/N_2O can be derived for March 19–22, 2003 for the incipient vortex (see Figure 10, panel a, black line). In the case of HNO_3, two reference functions were developed, one valid for altitudes above about 500 K – that is between the 30 and 125 ppbv N_2O level – and a second for altitudes below about 500 K – that is between the 125 and 300 ppbv N_2O level. Using empirical polynomial functions to describe the HNO_3/N_2O relationship, the best fit was derived by separating the relationship into two N_2O intervals.

Between March 19 and 22, Figure 10, panel a, and April 1 and 14, Figure 10, panel b, an increase in HNO_3 mixing ratios is observed at all observed equivalent latitudes for $N_2O < 150$ ppbv (below 500 K). The increase of HNO_3 likely occurs in accordance with decreasing NO_x owing to decreasing solar illumination at high latitudes as was observed for the Antarctic winter 1997 (see Section 4, below).

Between April, panel b, and the end of May, panel e, in Figure 10, HNO_3 mixing ratios increase from 12 ppbv to 15 ppbv above the 80 ppbv N_2O level (above 550 K). The largest increases occur poleward of 75°S equivalent latitude (Figure 10, panel e). HNO_3/N_2O profiles in April separate smoothly as a function of equivalent latitude up to mid-May in Figure 10, panel d. With decreasing sunlit hours per day

at lower latitudes, HNO_3 builds up during the second part of May. HNO_3 mixing ratios for different equivalent latitudes indicate a rather strong scatter above the 80 ppbv N_2O level.

However, a few observations between 70°Sand 75°S scatter significantly below the reference function at altitudes between 50 and 150 ppbv N_2O level (between 450 and 600 K). The first STS particles were detected at the end of May by MIPAS (ENVISAT) [*Spang et al.*, 2005; *Tilmes et al.*, 2006b] and may have absorbed gaseous HNO_3, which would result in decreasing HNO_3 mixing ratios. Correspondingly, ILAS-II aerosol extinction coefficients increase at this time of the year.

3.3. Local ozone loss using the CLaMS box model

Box model simulations with the Chemical Lagrangian Model of the Stratosphere (CLaMS) were performed to aid the interpretation of the ILAS-II measurements and to calculate chemical ozone loss in the setup phase of the 2003 Antarctic vortex. The model is described in detail by *McKenna et al.* [2002b, a]. Here, we use the CLaMS modules for trajectory and chemistry calculations. The reaction rates are used according to *Sander et al.* [2003]. The trajectories are calculated using MetO meteorological analyses. The diabatic vertical motion is calculated using the radiation scheme described by *Morcrette* [1991] and *Zhong and Haigh* [1995]. For the period from March 20 to May 31 2003, ten representative single air parcel trajectories are selected out of 3100 trajectories initialized at 600 and 650 K such that the considered air parcels stay close to a given latitude. The average latitudes of these trajectories are 60°S, 65°S, 70°S, 75°S, and 82°S for both levels.

Chemical tendencies along the trajectories are calculated within CLaMS. The initial chemical composition of the air parcels is derived from the average mixing ratio of 15 ILAS-II profiles (N_2O, Ozone, and HNO_3) obtained on March 20 and 21 at equivalent latitudes poleward of 75°S. H_2O and CH_4 are taken from a climatology (monthly means) based on HALOE data [*Grooß and Russell*, 2005].

Total inorganic chlorine (Cl_y) is derived from a relation with CH_4, derived from observations on board the ER-2 aircraft in spring 2000 [*Grooß et al.*, 2002] and total inorganic nitrogen (NO_y) from a correlation with N_2O, derived form in-situ observations in the 2002–03 Arctic winter [*Grooß et al.*, 2004]. N_2O_5 is set to 0.15 ppb and NO_x is assigned to the difference between HNO_3 + 2× N_2O_5 and NO_y. The obtained NO_x mixing ratios (3.8 ppb and 5.3 ppb at 600 and 650 K, respectively) are consistent with the HALOE climatology [*Grooß and Russell*, 2005] (3.1±1.3 ppb and 4.9±1.5 ppb, respectively). Total inorganic bromine (Br_y) is set to 22 ppt [*Sinnhuber et al.*, 2002]. These simulations were performed to investigate the latitude dependence of ozone depletion during the time of vortex formation. Further, other chemical aspects like the interaction between NO_x and HNO_3 were investigated with this simulation.

Figure 11.

Figure 11 shows the simulated ozone concentration along the five trajectories initialized on the isentropic levels 650 K (top panel) and 600 K (bottom panel) corresponding to mixing ratios of 74±4 ppbv and 97±5 ppbv N_2O, respectively. In the first weeks of the simulation, the net ozone depletion rate is largest for the most poleward trajectories. This is the case because ozone production rates and ozone loss rates depend differently on solar zenith angle. For lower solar elevation at polar latitudes, no significant ozone production by oxygen photolysis can occur while ozone loss cycles are still active [*Kawa et al.*, 2002]. In mid-April, the most poleward trajectory enters the polar night and therefore ozone depletion ceases. Trajectories further equatorward require more time to enter the polar night and, therefore, air parcels are characterized by a longer period of large solar zenith angles, compared to the most poleward trajectory. Therefore, ozone depletion is smallest at the most poleward trajectory, as shown in Figure 11, purple line. The simulated ozone depletion is larger for altitudes corresponding to 74 ppbv N_2O level (≈ 580 K in mid-April, 2003) than for the 97 ppbv level (≈ 540 K at mid-April, 2003) owing to larger NO_2 values at higher altitudes.

Contributions from different catalytic cycles are leading to the simulated

chemical ozone loss. For both altitudes considered, simulated ozone depletion is dominated by NO_x-catalyzed cycles. The fraction of NO_x-catalyzed ozone loss in the sum of all ozone loss cycles in early April is 64% to 78% for the trajectories starting at 650 K and 56% to 69% for the trajectories starting at 600 K. Also, the fraction of ozone loss due to NO_x-catalyzed cycles increases from 60°S poleward. **Figure 12.**

The ozone loss determined using CLaMS is now compared with the estimates derived from ILAS-II observations using the tracer correlation for all profiles measured inside the core of the entire vortex, as defined above (Figure 12). The ozone loss is calculated for all profiles measured by ILAS-II inside this region. The error bars correspond to the standard deviation of the daily averaged ozone loss. ILAS-II observations did not sample the very low ozone concentrations in March measured by MIPAS that are at most 0.2 ppmv smaller at the 600 K level and 0.1 ppmv at the 650 K level compared to lowest concentrations at ILAS-II locations, as described above. Therefore, in the calculation of chemical ozone loss, we correct for the effect of the different sampling of ozone-poor areas by ILAS-II in March and April by decreasing the apparent chemical ozone loss in April by 0.2 ppmv and 0.1 ppmv at the 74 ppbv and 97 ppbv N_2O level, respectively. Indeed, the purpose of this calculation is to give a rather rough estimate of chemical ozone loss for comparison with CLaMS simulations.

The averaged ozone loss between 580–620 K (corresponding to $\approx$ 74 ppbv N_2O and the 650 K level in March) for the period April 2 to 7 derived from ILAS-II measurements is 0.12 ppmv with a standard deviation of 0.17 ppmv ($\approx$ 5% of the availabe ozone). At lower altitudes, at 530–570 K (corresponding to $\approx$ 97 ppbv N_2O) ozone loss for the same time interval is 0.10 ppmv with a standard deviation of 0.17 ppmv, which is even less than 5% chemical ozone loss. The simulated ozone loss of 0.15 ppmv at the 74 ppbv N_2O level and of 0.08 ppmv at the 97 ppbv level is in good agreement with the values derived from the ILAS-II measurements within the variability of the deduced ozone loss. However, owing to the inhomogeneity of ozone concentrations with the inner vortex edge, the uncertainty of derived

chemical ozone loss is large, for example on April 8 and 9. In summary, from this analysis there is no indication of any problem with the NO_x chemistry for large solar zenith angles.

Figure 13.

Additionally, on both levels, simulated and measured HNO_3 agree quite well both in the absolute mixing ratios and in the temporal development of the conversion from NO_x to HNO_3 (see Figure 13).

4. Tracer/N_2O development during the setup phase of the 1997 Antarctic vortex

Figure 14.

The Antarctic polar vortex in winter 1997 started developing in March 1997, according to the definition from Section 3. An inner vortex edge exists during March at very high equivalent latitudes (85°S) at altitudes between 475 and 650 K, however the maximum $\nabla PV \cdot v$ is below 22.8 PVU/degrees*m/s. Therefore, the vortex is likely permeable up to the end of March 1997. During April, the inner vortex edge moves towards 75°S. In the first half of April, an outer and inner vortex exist at altitudes above 475 K. The maximum $\nabla PV \cdot v$ exceeds the threshold value for an isolated vortex at this time. In the second half of April and May, only the outer vortex edge is moving from 75°S to 65°S by the end of May at all altitudes considered. The inner vortex boundary is also found intermittently during May 1997.

In Table 1 the averaged solar illumination in sunlit hours per day averaged over certain time intervals and equivalent latitudes is shown at 550 K for both 2003 and 1997. During April 1997, there are slightly fewer averaged sunlit hours per day than during April 2003 for equivalent latitudes between 70°S and 80°S (see Table 1). However, significantly larger values for sunlit hours per day occur in April 1997 compared to April 2003 at equivalent latitudes between 80°S and 90°S, especially in late April. The larger illumination of equivalent latitudes poleward of 80°S in April 1997 is likely a result of a shift of the polar vortex towards lower geographical latitudes in this year.

Figure 15.

In the period March 16 to 30, 1997, the ILAS instrument only performed measurements within equivalent latitudes between 80°Sand 90°S (see Figure 15, panel a, pink squares). These O_3/N_2O profiles are located within the inner vortex core poleward of 85°S equivalent latitudes and show a compact relationship, whereas the other O_3/N_2O profiles show a strong scatter at altitudes above the 150 ppbv level of N_2O ($\approx$ 500 K). At this time, only an inner vortex edge exists at $\approx$85°S and thus there is no transport barrier between mid-latitudes and the outer vortex. It has to be noted that between 120 and 150 ppbv N_2O a small number of profiles scatter below this relation in March 1997 with a maximum deviation of 0.4 ppmv.

During the first half of April, ozone mixing ratios inside the inner vortex are up to 0.7 ppmv smaller at altitudes above 480 K (i.e. the 100 ppbv N_2O level) compared to values describing the reference function at the same equivalent latitudes. This may be a result of the different sampling of an inhomogeneous incipient vortex distribution and chemical ozone loss as described for winter 2003 (see Section 3.3).

The profiles measured inside the entire vortex poleward of 75°S in the first half of April are up to 2 ppmv larger compared to observations inside the partly isolated inner vortex. The ozone mixing ratios measured in the outer vortex decrease between March and April, possibly due to a combination of the increasing isolation of the entire vortex and ongoing chemical ozone loss. During the second half of April, only one vortex edge is established at an equivalent latitude of $\approx$ 75°S. Therefore, air masses poleward of $\approx$ 75°S mix within the entire vortex. This is why ozone mixing ratios in the inner and outer vortex (see Figure 15, panel c, large and small diamonds) are not separated anymore. A possible further decrease in ozone, owing to the solar illumination during late April, is masked by isentropic mixing between outer and inner vortex air.

During May 1997, the low ozone mixing ratios below 2 ppmv vanish owing to mixing within the vortex for equivalent latitudes equatorward of 85°S. No

measurements were obtained at equivalent latitudes poleward of 85°S since the beginning of May 1997. At this time of the year, the separation between observations inside the inner vortex and the entire vortex is still clear. The difference between observations inside the inner vortex and the outer vortex in May 1997 is larger than in May 2003 because in 1997 the transport barrier at the inner vortex edge might be still present during May (see Figure 14). During June 1997, the ozone-tracer correlations inside the entire vortex become uniform (Figure 15, panels f and g). An early winter reference function for the calculation of chemical ozone loss in spring can be derived for June 1997 to derive chemical ozone loss for the entire 1997 Antarctic winter as done by *Tilmes et al.* [2006a].

Figure 16.

The incipient vortex reference functions for NO_2/N_2O and HNO_3/N_2O are derived from all ILAS observations at high southern latitudes during the second half of March 1997 (Figure 16, black lines). Although NO_2 has a strong diurnal cycle, it is possible to consider the tracer-tracer relations of NO_2/N_2O, because ILAS measurements are taken always at the same solar zenith angle, namely at sunset in the Antarctic.

During the second half of March the NO_2/N_2O and HNO_3/N_2O correlations are very uniform and compact (Figure 16, black lines). In contrast, the O_3/N_2O correlations show a rather large scatter (Figure 15, panel a). At this time of the year, the entire area between 55°S and 90°S is highly illuminated, see Table 1, and therefore no strong meridional gradients in HNO_3 and NO_2 exist. Indeed, NO_2 is short-lived and will adjust to the photochemical equilibrium quickly. During April, HNO_3 mixing ratios increase by up to 5 ppbv and NO_2 mixing ratios decrease by $\approx$ 3-4 ppbv. Note that in correspondence with increasing HNO_3, NO_x (that is defined $NO_x = NO_2 + NO$) is decreasing. Therefore, the NO_2 decrease must be less than the HNO_3 increase. The scatter in NO_2/N_2O profiles increases (Figure 16, bottom left panel) because the profiles may reflect different amounts of solar illumination received, depending on their location. As long as some NO_x is left, NO_x-catalyzed cycles are still effective, which is the case during the second part of April 1997.

4.1. Comparison of the tracer development during the setup phase of 1997 and 2003 Antarctic vortices

The vortices in both Antarctic winters 1997 and 2003 started forming in March according to the *Nash et al.* [1996] criterion. In 1997, an inner vortex boundary formed at very high equivalent latitudes. In 2003, a vortex edge was detected at equivalent latitudes around 75°S. The different evolution of the Antarctic polar vortex in March 1997 compared to March 2003 (compare Figures 1 and 14) results in different tracer-tracer correlations for the two incipient vortices. The smaller vortex in March 1997 than in March 2003 results in a strong variability of ozone mixing ratios in March 1997 at equivalent latitudes equatorward of 80°S. Although the maximum $\nabla PV \cdot v$ is not very large (most of the time below 22.8 PVU/degrees*m/s), the inner vortex in March 1997 at very high latitudes seems to be isolated at this time of the year, because of a compact O_3/N_2O relationship very close to the pole (see Figure 15 panel a). In both years, HNO_3/N_2O (see Figure 10, panel a, and Figure 16, left panels, black line) (NO_2/N_2O only for 1997) scatter plots are compact within the entire polar region in March.

In the first part of April, a partially isolated inner vortex core exists inside the vortex during both years. O_3/N_2O correlations indicate significantly lower ozone concentrations inside the inner polar vortex compared to the outer vortex. A maximum deviation from the incipient reference function of up to ≈ 0.7 ppmv is found at this time for both years. The mixing ratios of HNO_3 during April and May are slightly different in 1997 and 2003. HNO_3 increases less at altitudes above ≈ 540 K in 1997 compared to 2003. In May, HNO_3 does not reach mixing ratios of more than 15 ppbv inside the vortex core as was observed at the end of May 2003 (not shown for 1997).

Further, the O_3/N_2O correlations in June 1997 show larger ozone mixing ratios above the 150 N_2O level compared to June 2003. These larger ozone mixing ratios in 1997 are apparent within the vortex by May. A likely reason for this is a weaker transport barrier at the outer vortex edge during the setup phase in winter 1997

than in winter 2003, compare Figures 1 and 14. This results in a stronger increase of ozone in 1997 than in 2003 due to mixing of extra vortex air masses into the vortex before June. Thus, the shape of the tracer-tracer relationship in June is not the same for these two years, because it depends on the dynamical development of the incipient vortex.

5. Tracer/N_2O development during the setup phase of the early Arctic vortex 2003

For the Arctic winter 2003–04, observations during the setup phase of the vortex are available from ILAS-II. Figure 17 shows that the Arctic vortex in 2003 started forming at the end of September 2003 at altitudes above 550 K. At this time, a very weak vortex edge is determined for equivalent latitudes poleward of 70°N. Since October, the pattern of $\nabla PV \cdot v$ indicates the existence of both an inner and an outer transport barrier at 650 K at 60°N and 70°N equivalent latitude and partly in lower altitudes at the beginning of November. Since November, a vortex edge is observed almost continuously between 550 and 650 K at ≈ 60°N equivalent latitude.

Figure 17.

Although no ILAS-II measurements are available after October 24, 2003, the setup phase of the Arctic vortex can be investigated. During the end of September and October 2003 (corresponding to March and April in the SH), measurements were obtained inside the inner vortex edge or entire vortex edge at altitudes between 550 and 650 K. ILAS-II was measuring at ≈ 70°N, and the early vortex was located poleward 75°N. Therefore, only a few measurements within the Arctic incipient vortex were obtained.

Figure 18.

A large variability in O_3/N_2O correlations is observed in September 2003 between the 50 to 150 ppbv N_2O level (≈ 500-700 K) (see Figure 18, panel a) – like in the Antarctic vortex (Figure 15, panel a). At the beginning of October, profiles measured within the inner vortex core poleward of 75°N show a compact O_3/N_2O relationship that is used to derive an incipient vortex reference function

(see Figure 18, black line, all panels), although the transport barrier at the inner vortex edge seems to be weak (Figure 17). As for the Antarctic, a separation between inner and outer vortex profiles is noticeable especially at altitudes above the 80 ppmv N_2O level, in accordance with the existence of two vortex transport barriers above 550 K at this time. A minimum of ozone occurs poleward of 80°N at the 130 ppbv N_2O level.

Small ozone concentrations of the incipient Antarctic vortex 2003 and 1997 (during April) occur exactly at the corresponding time of the Arctic early winter 2003 (during October). As described for the setup phase of the 1999 Arctic vortex, chemical, NO_x driven ozone depletion reduces ozone concentrations at this time of the year [*Kawa et al.*, 2002]. The large variability of inner vortex profiles indicates the inhomogeneous distribution of ozone mixing ratios with the incipient vortex. During October 21-24, 2003, profiles withing the inner vortex are more compact than during the first half of October (Figure 18, panel c). At this time, the inner vortex edge is stronger and has developed over the entire altitude range between 475 and 550 K.

The tracer-tracer correlations of HNO_3/N_2O at the end of September 2003 in high northern latitudes are compact, similar to the tracer-tracer correlations at high southern latitudes at the end of March. The derived reference for late September 2003 and the range of uncertainty – that is described by the standard deviation of the profiles – within the vortex is shown in Figure 19, black line. The increase in HNO_3 between the end of September and early October (black line compared to colored diamonds in Figure 19, left panel) in the Arctic is significantly smaller than the increase observed in the Antarctic. Further, there is less variation between profiles inside the vortex core and the outer vortex in the Arctic than in the Antarctic. This is in agreement with the fact that the sunlit hours per day differ by up to 8 hours per day between 90°S and 55°S equivalent latitude for the 2003 Antarctic winter with very little sunlit hours per day close to the pole (see Table 1). For the Arctic, the variability of sunlit hours for different equivalent

latitudes is less strong and the number of sunlit hours per day is larger, likely because the Arctic vortex moves more often towards lower latitudes during this time of the year compared to the Antarctic vortex. At the end of October/April the conditions in both hemispheres are more similar. **Figure 19.**

6. Conclusions

Ozone concentrations in the incipient Antarctic and Arctic polar vortex show large variations (between 2 and 4 ppmv). Meteorological analyses and tracer-tracer correlations indicate a separation of the incipient polar vortex into an inner vortex that is noticeably isolated from an outer vortex by a transport barrier. During the setup phase of the vortex, the outer vortex is influenced by mixing with air from mid-latitudes, which increases ozone mixing ratios. Inside the isolated inner vortex ozone mixing ratios show a variability of ≈ 0.5 ppmv within the same equivalent latitude bin. Patches of very low ozone are observed by MIPAS (ENVISAT) already in March. The lowest ozone mixing ratios observed by ILAS and ILAS-II are during early April, 1.7 ppmv (Antarctic), and the first half of October, 1.8 ppmv (Arctic) in the inner vortex at 500–550 K. This corresponds exactly to the time when the vortex becomes isolated at these altitudes and when the solar illumination decreases. In accordance with the mechanism described by *Kawa et al.* [2002], we find net ozone destruction during the first weeks of April (Antarctic) and October (Arctic), owing to decreasing solar illumination.

CLaMS box model simulations indicate that moderate chemical ozone loss during the times considered here is mainly caused by NO_x-catalyzed cycles. The conversion between NO_x and HNO_3 observed in ILAS measurements is in good agreement with box model simulations. The rough estimation of chemical ozone loss using ILAS-II observations during the first week of April in the Antarctic winter 2003 is also in agreement with box model simulations.

In the Antarctic at the end of April no ozone loss is detected within the inner vortex corresponding to the lack of sunlight in high polar latitudes (poleward of

80°S). From that time onward, the transport barrier between the inner and outer vortex vanishes and ozone becomes uniform inside the entire vortex through mixing. During June, the ozone-tracer correlations become uniform for profiles located within the entire vortex and ozone loss stops within the entire vortex, because of the lack of sunlight. At this time, an early winter reference function is derived to calculate chemical ozone loss in spring [*Tilmes et al.*, 2006a]. The exact shape of the early winter reference function depends on the extent of vortex isolation during the setup phase of the polar vortex.

Acknowledgments. We gratefully acknowledge all members of the science team of the Improved Limb Atmospheric Spectrometer (ILAS and ILAS-II) led by Dr. Y. Sasano and Dr. H. Nakajima for processing ILAS (V6.0) and ILAS-II (V1.4) data. ILAS and ILAS-II were developed by the Ministry of the Environment, Japan (MOE) and was aboard the ADEOS and ADEOS-II satellite launched by the Japan Aerospace Exploration Agency (JAXA). ILAS and ILAS-II data were processed at the ILAS and ILAS-II Data Handling Facility, National Institute for Environmental Studies (NIES). Thanks are also due to the European Space Agency for providing MIPAS data and the UK Meteorological Office for providing meteorological analyses. We further thank Janet Carter-Sigglow for a grammatical and stylistic revision of the manuscript and S. Tilmes thanks the Deutsche Akademie der Naturforscher Leopoldia and the Bundesministerium für Bildung und Forschung for supporting this study.

References

Brühl, C., P. J. Crutzen, and J.-U.Grooß (1998), High-latitude, summertime NOx activation and seasonal ozone decline in the lower stratosphere: Model calculations based on observations by HALOE on UARS, *J. Geophys. Res.*, *103*(D3), 3587–3597.

Crutzen, P. J. (1970), The influence of nitrogen oxides on the atmospheric ozone content, *Q. J. R. Meteorol. Soc.*, *96*, 320–325.

Crutzen, P. J., and C. Brühl (2001), Catalysis by NOx as the main cause of the spring to fall stratospheric ozone decline in the northern hemisphere, *J. Phys. Chem. A*, *105*, 1579–1582.

Ejiri, M. K., et al. (2006), Validation of ILAS-II V1.4 nitrous oxide and methane profiles, *J. Geophys. Res.*, submitted.

Fahey, D. W., and A. R. Ravishankara (1999), Summer in the stratosphere, *Science*, *285*, 208–210.

Farman, J. C. (1985), Ozone photochemistry in the Antarctic stratosphere in summer, *Q. J. R. Meteorol. Soc.*, *111*, 1013–1025.

Farman, J. C., B. G. Gardiner, and J. D. Shanklin (1985), Large losses of total ozone in Antarctica reveal seasonal ClO_x/NO_x interaction, *Nature*, *315*, 207–210.

Fischer, H., and H. Oelhaf (1996), Remote sensing of vertical profiles of atmospheric trace constituents with MIPAS limb-emission spectrometers, *Appl. Opt.*, *35*, 2787–2796.

Grooß, J.-U., and J. M. Russell (2005), Technical note: A stratospheric climatology for O_3, H_2O, CH_4, NO_x, HCl and HF derived from HALOE measurements, *Atmos. Chem. Phys.*, *5*, 2797–2807.

Grooß, J.-U., G. Günther, R. Müller, P. Konopka, S. Bausch, H. Schlager, C. Voigt, C. M. Volk, and G. C. Toon (2004), Simulation of denitrification and ozone loss for the Arctic winter 2002/2003, *Atmos. Chem. Phys.*, *4*, 8069–8101.

Grooß, J.-U., et al. (2002), Simulation of ozone depletion in spring 2000 with the Chemical Lagrangian Model of the Stratosphere (CLaMS), *J. Geophys. Res.*, *107*, 8295, doi:10.1029/2001JD000456.

Juckes, M., and M. McIntyre (1987), A high resolution, one-layer model of breaking planetary waves in the stratosphere, *Nature*, *328*, 590–596.

Kanzawa, H., et al. (2003), Validation and data characteristics of nitrous oxide and methane profiles observed by the the Improved Limb Atmospheric Spectrometer (ILAS) and processed with the Version 5.20 algorithm, *J. Geophys. Res.*, *108*, 8003, doi:10.1029/2002JD002458.

Kawa, S. R., R. M. Bevilacqua, J. J. Margitan, A. R. Douglass, M. R. Schoeberl, K. W. Hoppel, and B. Sen (2002), Interaction between dynamics and chemistry of ozone in the setup phase of the Northern Hemisphere polar vortex, *J. Geophys. Res.*, *107*, 8310, doi:10.1029/2001JD001527.

Kawamoto, M., H. Kanzawa, and M. Shiotani (2004), Time variations of descent in the antarctic vortex during the early winter of 1997, *J. Geophys. Res.*, *109*, doi:10.1029/2004JD004650.

Konopka, P., et al. (2004), Mixing and ozone loss in the 1999-2000 Arctic vortex: Simulations with the 3-dimensional Chemical Lagrangian Model of the Stratosphere (CLaMS), *J. Geophys. Res.*, *109*, D02315, doi:10.1029/2003JD003792.

Lait, L. R. (1994), An alternative form for potential vorticity, *J. Atmos. Sci.*, *51*, 1754–1759.

Lee, A., H. Roscoe, A. Jones, P. Haynes, E. Shuckburgh, M. Morrey, and H. Pumphrey (2001), The impact of the mixing properties within the Antarctic stratospheric vortex on ozone loss in spring, *J. Geophys. Res.*, *106*(D3), 3203–3212, doi:10.1029/2000JD900398.

Manney, G. L., R. W. Zurek, A. O'Neill, and R. Swinbank (1994), On the motion of air through the stratospheric polar vortex, *J. Atmos. Sci.*, *51*, 2973–2994.

McKenna, D. S., J.-U. Grooß, G. Günther, P. Konopka, R. Müller, G. Carver, and Y. Sasano (2002a), A new Chemical Lagrangian Model of the Stratosphere (CLaMS): Part II Formulation of chemistry-scheme and initialisation, *J. Geophys. Res.*, *107*(D15), 4256, doi:10.1029/2000JD000113.

McKenna, D. S., P. Konopka, J.-U. Grooß, G. Günther, R. Müller, R. Spang, D. Offermann, and Y. Orsolini (2002b), A new Chemical Lagrangian Model of the

Stratosphere (CLaMS): Part I Formulation of advection and mixing, *J. Geophys. Res.*, *107*(D16), 4309, doi:10.1029/2000JD000114.

Michelsen, H. A., G. L. Manney, M. R. Gunson, and R. Zander (1998), Correlations of stratospheric abundances of NO_y, O_3, N_2O, and CH_4 derived from ATMOS measurements, *J. Geophys. Res.*, *103*, 28,347–28,359.

Morcrette, J.-J. (1991), Radiation and cloud radiative properties in the European Centre for Medium-Range Weather Forecasts forecasting system, *J. Geophys. Res.*, *96*(D5), 9121–9132.

Müller, R., P. J. Crutzen, J.-U. Grooß, C. Brühl, J. M. Russel III, and A. F. Tuck (1996), Chlorine activation and ozone depletion in the Arctic vortex: Observations by the Halogen Occultation Experiment on the Upper Atmosphere Research Satellite, *J. Geophys. Res.*, *101*, 12,531–12,554.

Müller, R., S. Tilmes, P. Konopka, J.-U. Grooß, and H.-J. Jost (2005), Impact of mixing and chemical change on ozone-tracer relations in the polar vortex, *Atmos. Chem. Phys.*, *5*, 3139–3151.

Müller, R., et al. (2002), Chlorine activation and chemical ozone loss deduced from HALOE and balloon measurements in the Arctic during the winter of 1999-2000, *J. Geophys. Res.*, *107*, 8302, doi:10.1029/2001JD001423.

Nakajima, H., et al. (2005), Characteristics and performance of the Improved Limb Atmospheric Spectrometer-II (ILAS-II) onboard the ADEOS-II satellite, *J. Geophys. Res.*, submitted.

Nash, E. R., P. A. Newman, J. E. Rosenfield, and M. R. Schoeberl (1996), An objective determination of the polar vortex using Ertel's potential vorticity, *J. Geophys. Res.*, *101*, 9471–9478.

Perliski, L., S. Solomon, and J. London (1989), On the interpretation of seasonal-variations of stratospheric ozone, *Planet. Space Sci.*, *37*, 1527–1538.

Pierce, R. B., and T. D. Fairlie (1993), Chaotic advection in the stratosphere: Implication for the dispersal of chemically perturbed air from the polar vortex, *Geophys. Res. Lett.*, *98*, 18,589–18,595, doi:10.1029/93GL01619.

Proffitt, M. H., K. Aikin, J. J. Margitan, M. Loewenstein, J. R. Podolske, A. Weaver, K. R. Chan, H. Fast, and J. W. Elkins (1993), Ozone loss inside the northern polar vortex during the 1991-1992 winter, *Science*, *261*, 1150–1154.

Rosenfield, J. E., P. A. Newman, and M. R. Schoeberl (1994), Computations of diabatic descent in the stratospheric polar vortex, *J. Geophys. Res.*, *99*(D8), 16,677–16,689.

Russell, J. M., L. L. Gordley, J. H. Park, S. R. Drayson, A. F. Tuck, J. E. Harries, R. J. Cicerone, P. J. Crutzen, and J. E. Frederick (1993), The Halogen Occultation Experiment, *J. Geophys. Res.*, *98*, 10,777–10,797.

Sander, S. P., et al. (2003), *Evaluation number 14*, Chemical kinetics and photochemical data for use in atmospheric studies, NASA Panel for Data Evaluation, JPL Publication 02-25, Jet Propulsion Laboratory, California Insitute of Technology, Pasadena, California.

Sasano, Y., M. Suzuki, T. Yokota, and H. Kanzawa (1999), Improved limb atmospheric spectrometer (ILAS) for stratospheric ozone layer measurements by solar occultation technique, *Geophys. Res. Lett.*, *26*, 197–200, doi: 10.1029/1998GL900276.

Sinnhuber, B.-M., et al. (2002), Comparison of measurements and model calculations of stratospheric bromine monoxide, *J. Geophys. Res.*, *107(D19)*, doi:10.1029/2001JD000,940.

Solomon, S. (1999), Stratospheric ozone depletion: A review of concepts and history, *Rev. Geophys.*, *37*(3), 275–316, doi:10.1029/1999RG900008.

Spang, R., J. J. Remedios, S. Tilmes, and M. Riese (2005), MIPAS observation of polar stratospheric clouds in the Arctic 2002/3 and Antarctic 2003 winters, *Adv. Space. Res.*, *36*(5), 868878.

Steinhorst, H.-M., P. Konopka, G. Günther, and R. Müller (2005), How permeable is the edge of the Arctic vortex — Model studies of the winter 1999-2000, *J. Geophys. Res.*, *110*, D06105, doi:10.1029/2004JD005268.

Sugita, T., et al. (2006), Ozone profiles in the high-latitude stratosphere and lower mesosphere measured by the Improved Limb Atmospheric Spectrometer-II

(ILAS-II): Comparison with other satellite sensors and ozonesondes, *J. Geophys. Res.*, submitted.

Suzuki, M. A., A. Matsuzaki, T. Ishigaki, N. Kimura, N. Araki, T. Yokota, and Y. Sasano (1995), Ilas, the improved limb atmospheric spectrometer, on the advanced earth observing satellite, *IEICE TRANS Commun*, *E78-B,12*, 1560–1570.

Swinbank, R., and A. O'Neill (1994), A stratosphere-troposphere data assimilation system, *Mon Wea Rev*, *122*, 686–702.

Tilmes, S., R. Müller, J.-U. Grooß, D. S. McKenna, J. M. Russell, and Y. Sasano (2003), Calculation of chemical ozone loss in the Arctic winter 1996-1997 using ozone-tracer correlations: Comparison of Improved Limb Atmospheric Spectrometer (ILAS) and Halogen Occultation Experiment (HALOE) results, *J. Geophys. Res.*, *108*, 4045, doi:10.1029/2002JD002213.

Tilmes, S., R. Müller, J.-U. Grooß, and J. M. Russell (2004), Ozone loss and chlorine activation in the Arctic winters 1991–2003 derived with the tracer-tracer correlations, *Atmos. Chem. Phys.*, *4*(8), 2181–2213.

Tilmes, S., R. Müller, A. Engel, M. Rex, and J. M. Russell III (2006a), Chemical ozone loss in the Arctic and Antarctic stratosphere between 1992 and 2005, *Geophys. Res. Lett.*, accepted.

Tilmes, S., R. Müller, J.-U. Grooß, R. Spang, T. Sugita, H. Nakajima, and Y. Sasano (2006b), Chemical ozone loss and related processes in the Antarctic winter 2003 based on improved limb atmospheric spectrometer (ILAS)-II observations, *J. Geophys. Res.*, *111*, D11S12, doi:10.1029/2005JD006260.

Yokota, T., et al. (2005), Improved Limb Atmospheric Spectrometer-II (ILAS-II) version 1.4 algorithm for retrieval of gas and aerosol profiles in the stratosphere, *J. Geophys. Res.*, in preparation.

Zhong, W., and J. D. Haigh (1995), Improved broadband emissivity parameterization for water vapor cooling rate calculations, *J. Atmos. Sci.*, *52*(1), 124–138.

S. Tilmes, R. Müller and J.-U. Grooß, Forschungszentrum Jülich, Institute of

Stratospheric Research (ICG-I), 52425 Jülich, Germany (e-mail: tilmes@ucar.edu),
H. Nakajima and Y. Sasano, Nies, Japan

Received _____

Version of August 22, 2006

Figure Captions

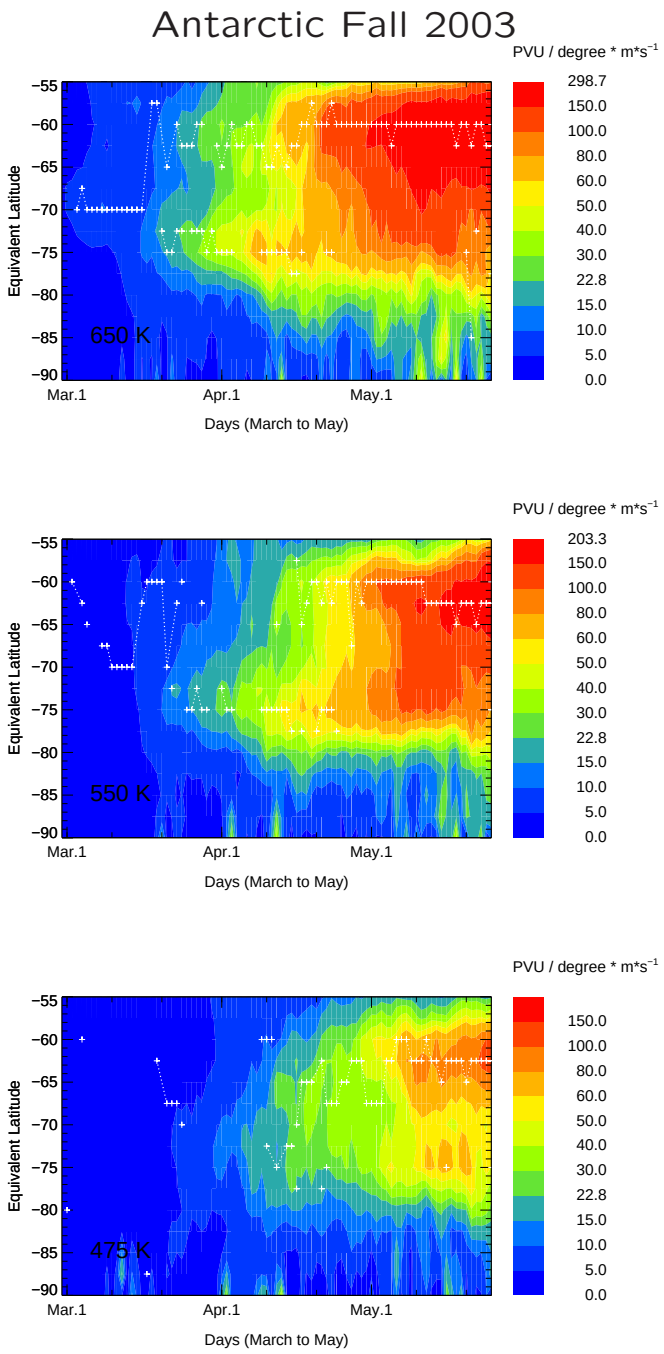

Figure 1. First derivative of the modified potential vorticity [*Lait*, 1994] (Θ_0 = 450 K) with respect to equivalent latitude times wind velocity are shown between March 1 and May 31, 2003 at different potential temperature levels, 650 K (top panel), 550 K (middle panel) and 475 K (bottom panel). White crosses indicate the inner and outer vortex edge determined using the *Nash et al.* [1996] criterion at the corresponding potential temperature level (see text). The changeover from blue to green colors illustrates the threshold value of 22.8 PVU/degree · m/s, at which the vortex can be assumed to be isolated (see text).

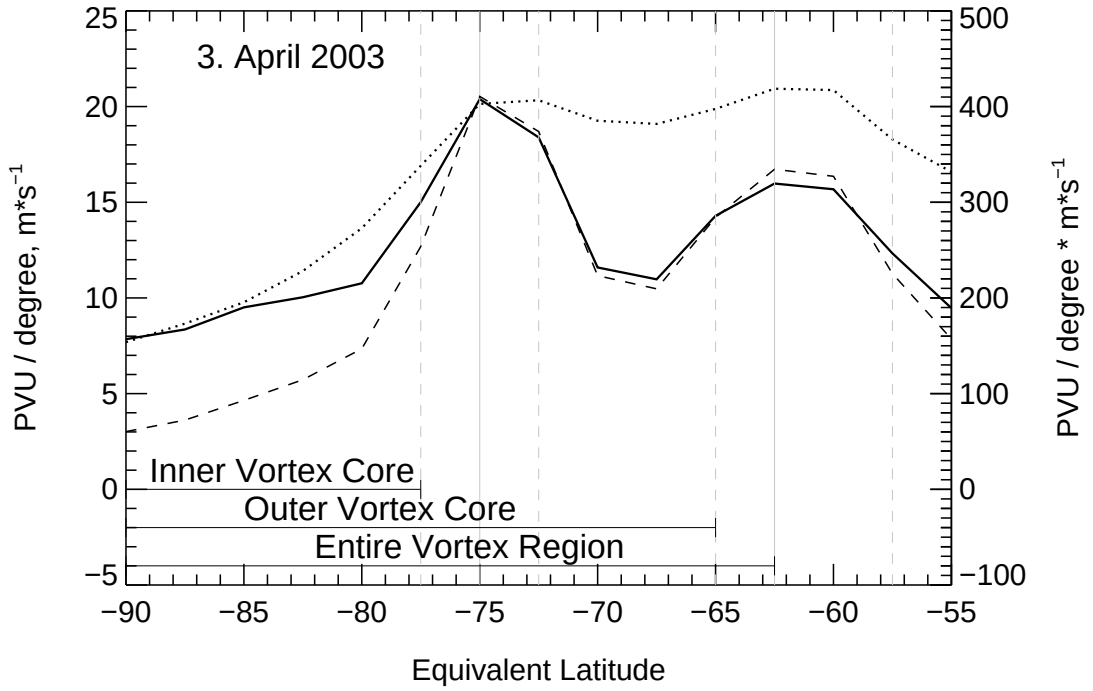

Figure 2. First derivative of potential vorticity (solid line), the wind velocity, v (mean meridional and zonal wind) (dotted line) and $\nabla PV \cdot v$ (dashed line), to equivalent latitude is shown for April 3, 2003 at 650 K potential temperature. Solid gray lines indicate the inner/outer/entire vortex edge determined using the *Nash et al.* [1996] criterion (see text). Dashed grey lines indicate the edge of the vortex boundary regions.

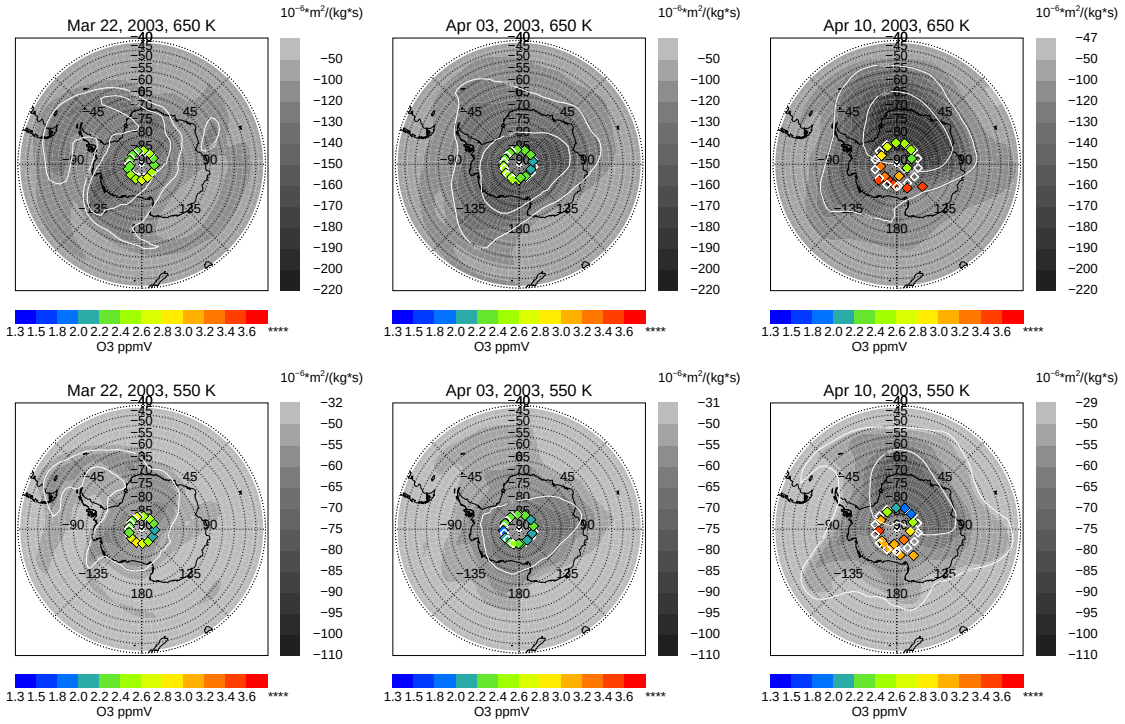

Figure 3. The potential vorticity derived from MetO data at the 650 K (top panel) and 550 K (bottom panel) potential temperature level valid for March 22, April 03 and April 10, 2003 12 UTC, shown on a grey scale. For the same Θ level, ozone mixing ratios in ppmv as derived from the satellite profiles are represented as colour-coded diamonds (ILAS). All satellite profiles were repositioned to 12 UTC by trajectory calculations. Also shown are the positions of satellite profiles at the time of measurement (different from 12 UTC) in white diamonds (ILAS).

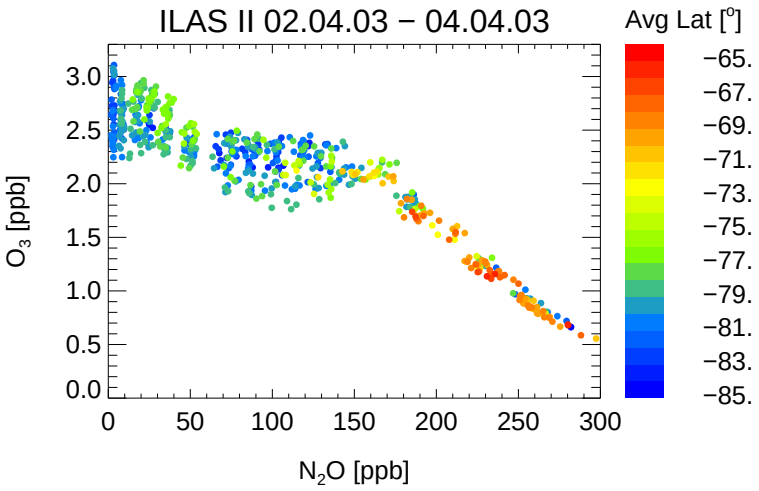

Figure 4. Ozone/N_2O correlations between April 2–4, 2003 within the inner vortex. Colors indicate the average equivalent latitude of back trajectories until March 10, 2003, starting at ILAS-II locations using the CLaMS trajectory module, as described in Section 3.3.

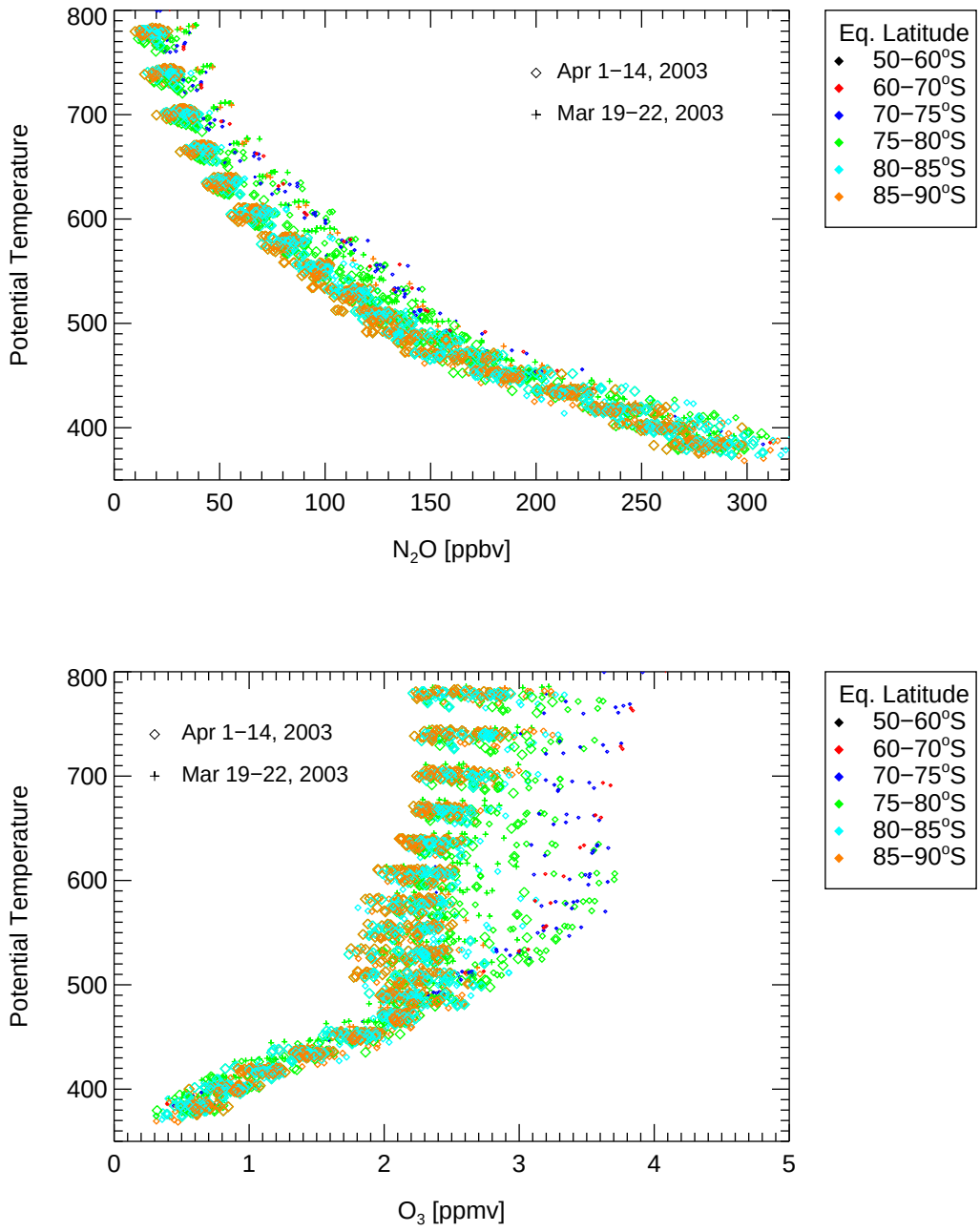

Figure 5. Ozone (top panel) and N_2O (bottom panel) profiles inside the early Antarctic vortex in 2003 for March 19–22 and April 1–14, 2003 from ILAS-II measurements. Different colors indicate different range of equivalent latitude of vortex profiles, as in Figure 8. Additionally, profiles outside the vortex are shown as black dots.

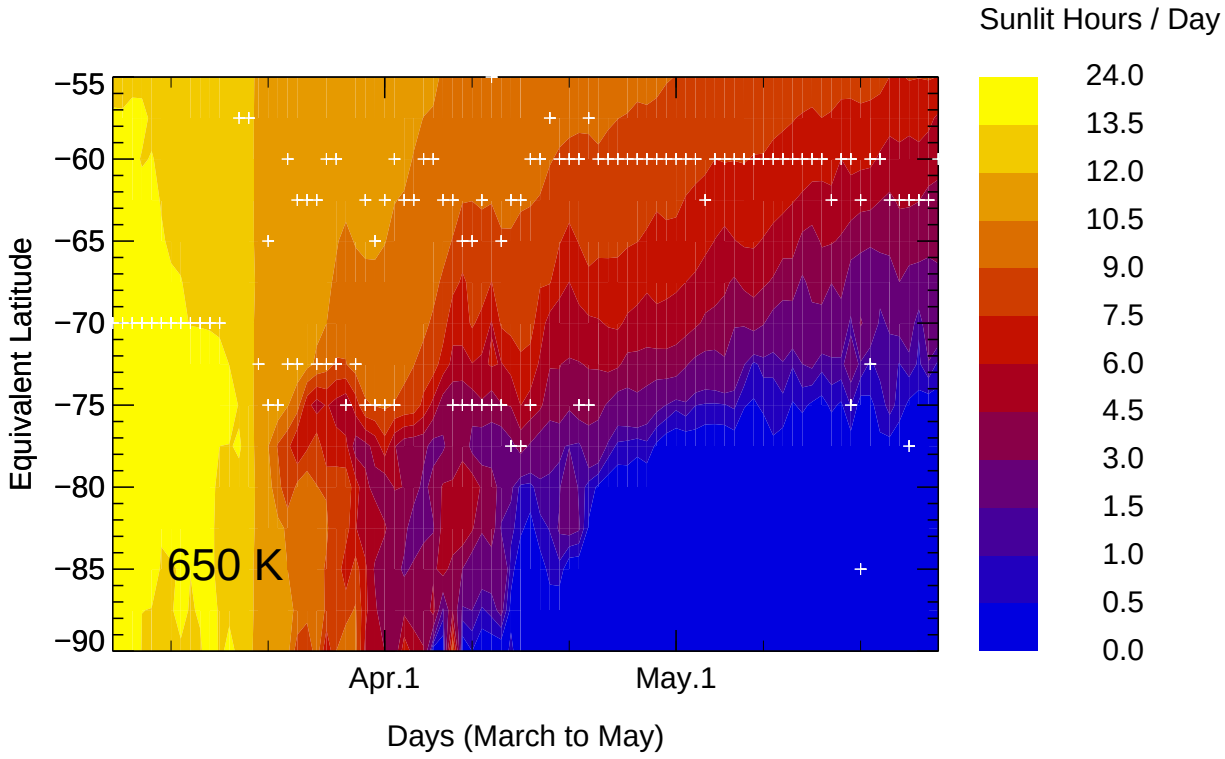

Figure 6. Sunlit hours per day are shown between March 1 and May 31, 2003 at the 550 K potential temperature level. White crosses indicate the inner and outer vortex edge determined using the *Nash et al.* [1996] criterion as in Figure 1.

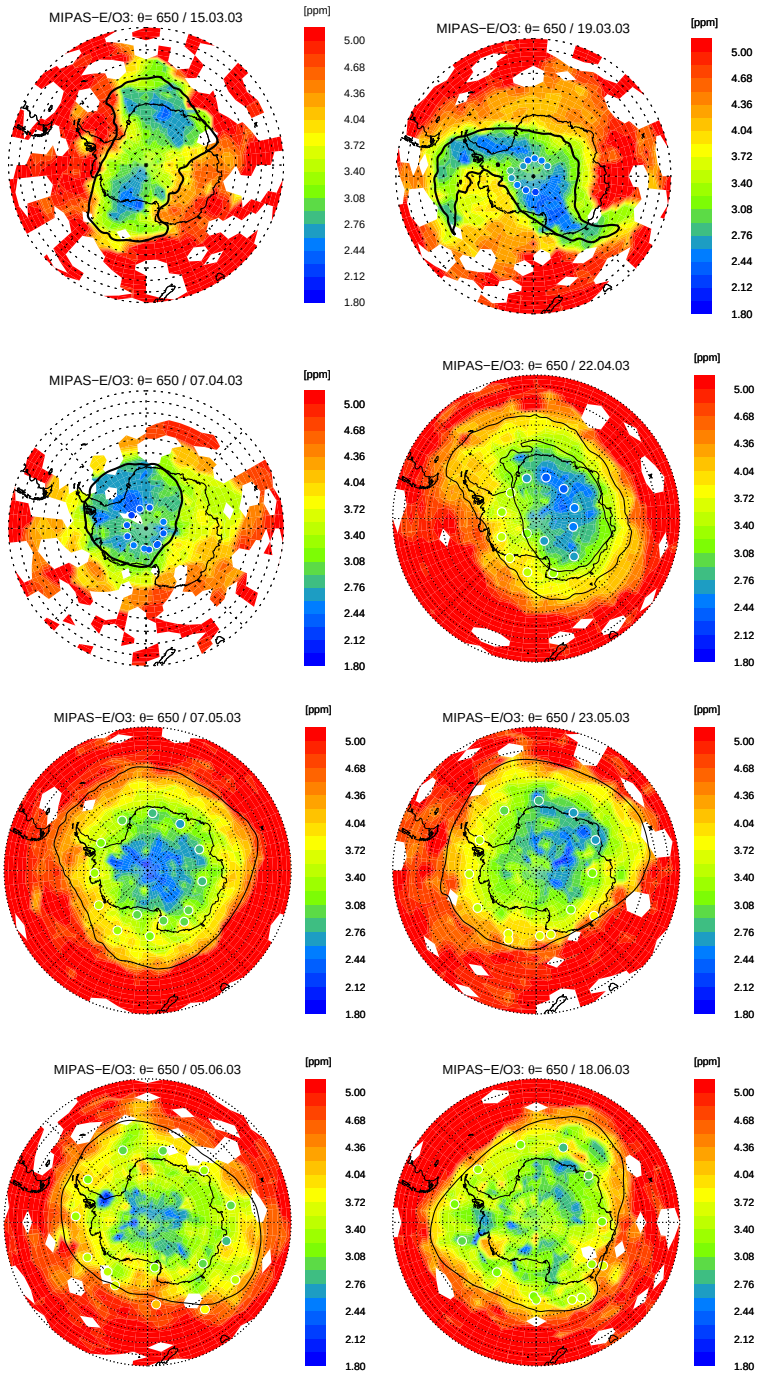

Figure 7. Composite of MIPAS data at the 650K potential temperature surface. The MIPAS data were collected within ± 2 days of the considered day (12 UT). The synoptic location of each data point is determined by forward and backward trajectories. These data are averaged onto a 2×6 degree regular grid using a cosine square distance weighting. Overlaid on this plot are the corresponding ILAS-II locations and values as colored circles with white edges. White areas correspond to no available data. The ozone mixing ratios exceed 5 ppm in the red areas. Further, the vortex edge (see text) is shown as a solid black line.

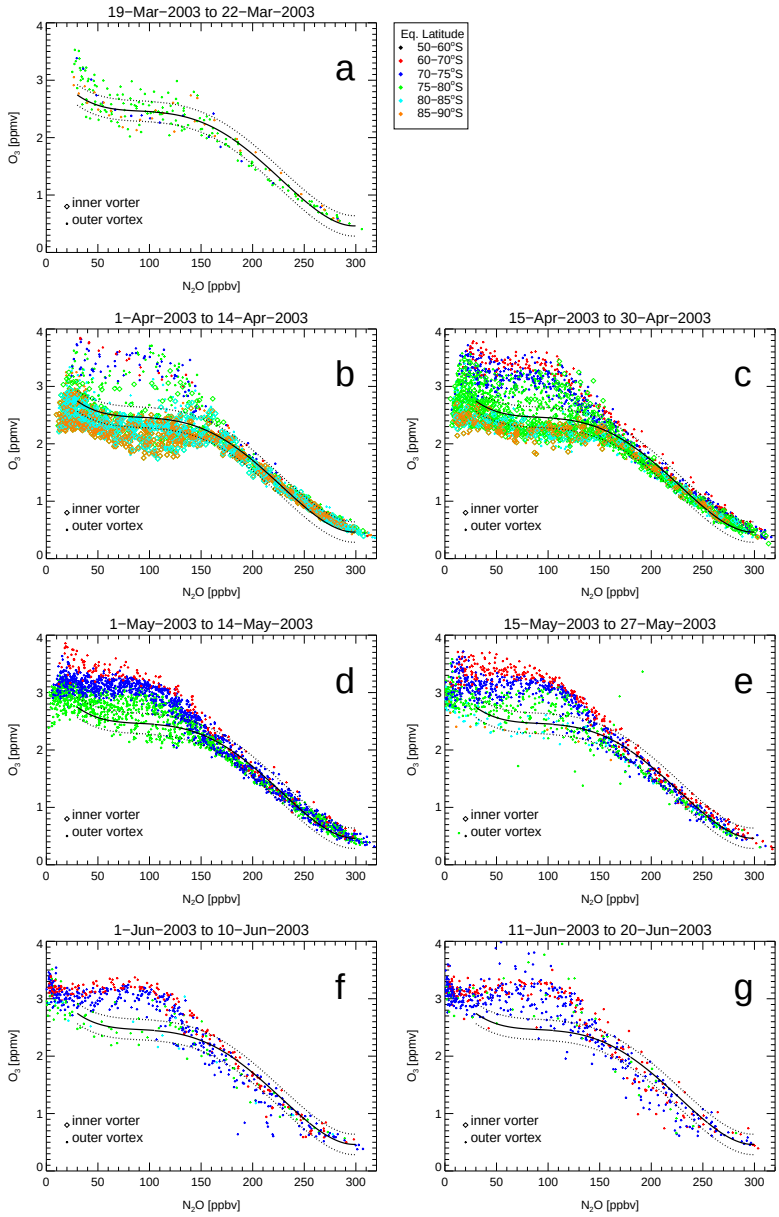

Figure 8. O_3/N_2O relation inside the early Antarctic vortex in 2003 prior to polar night from ILAS-II measurements for March 19-22 (panel a), April 1-14 (panel b), April 15-30 (panel c), May 1-14 (panel d), May 15-27 (panel e), June 1-10 (panel f), June 11-20 (panel g). Black line shown in each panel is a reference function derived as an empirical polynomial fit (Eq.1) for March 19–22, 2003 (panel a) with the area of uncertainty derived from the standard deviation of the profiles (dotted lines). Different colors indicate different range of equivalent latitude of vortex profiles, see panel a and text.

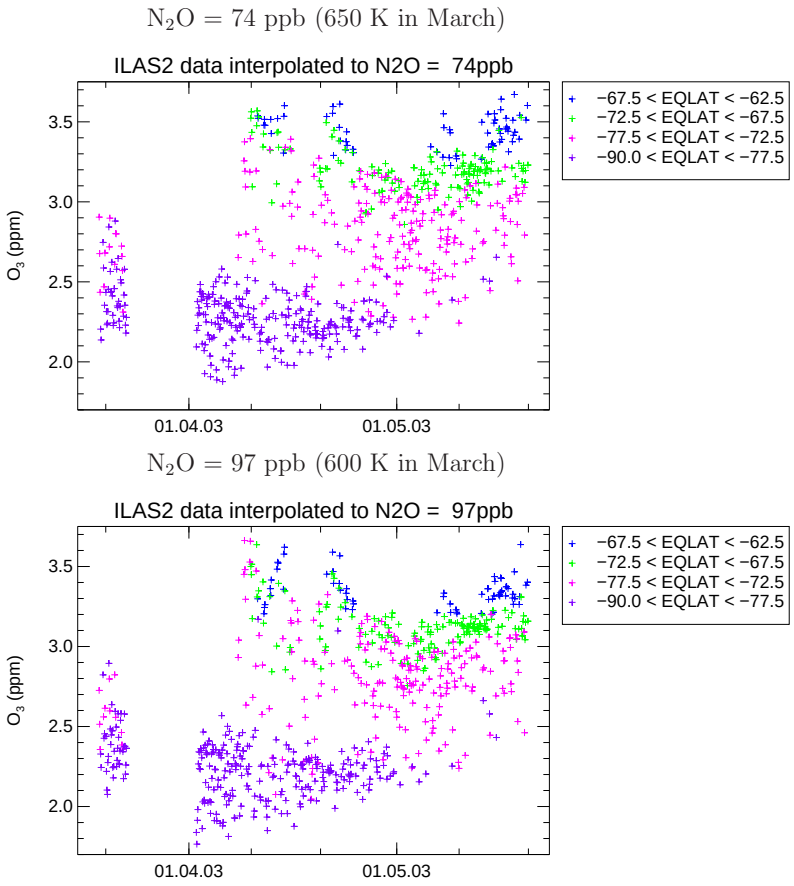

Figure 9. O_3 mixing ratios in different equivalent latitude regions (colored plus signs), between March 19 and May 31, 2003, measured by the ILAS-II instrument.

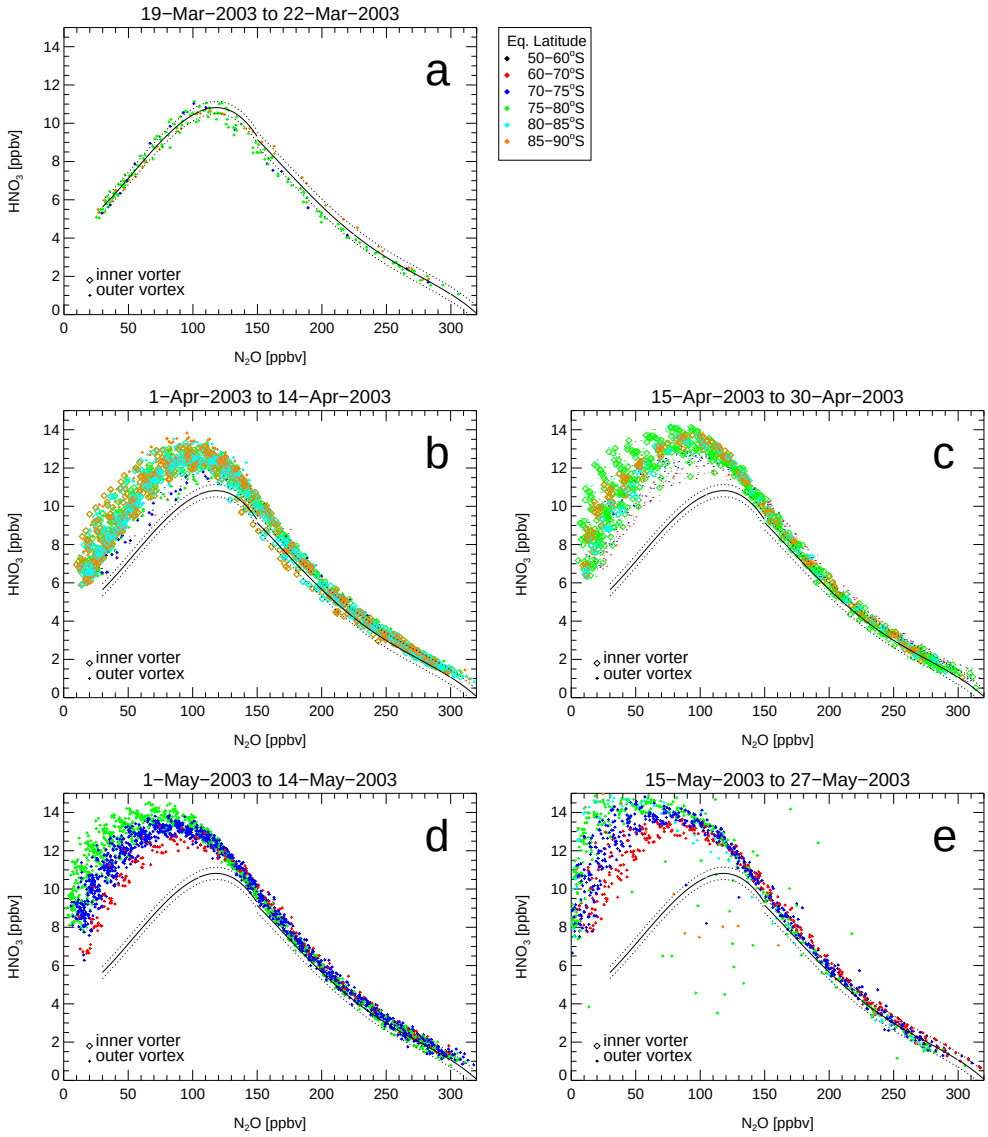

Figure 10. As Figure 8, but for HNO_3/N_2O, and without data for June (panels f and g).

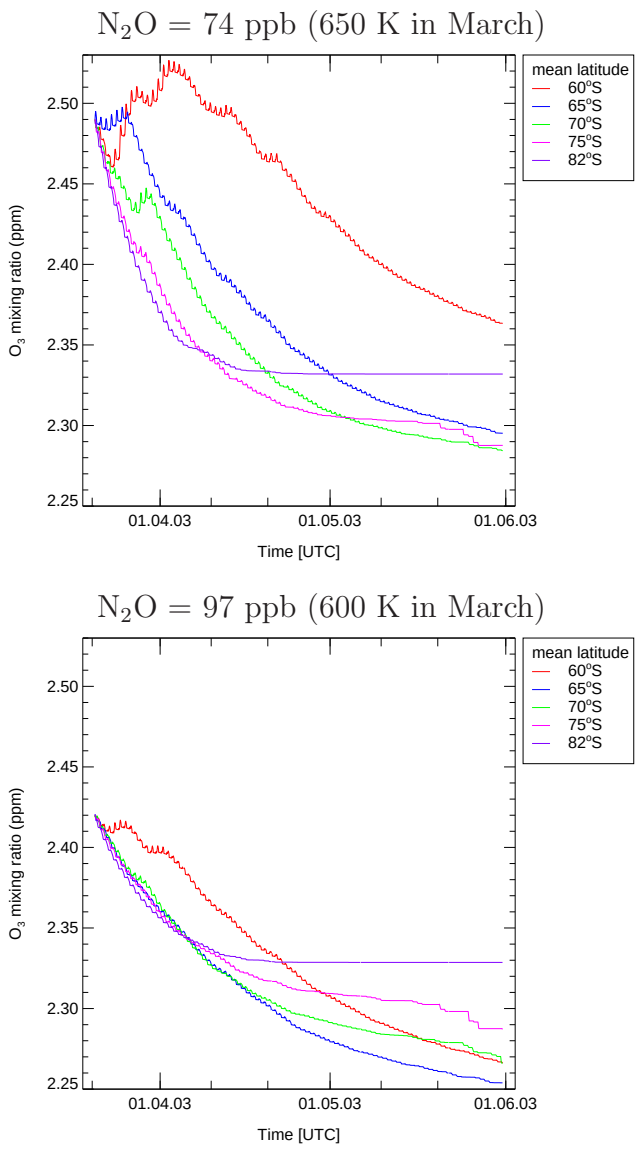

Figure 11. Simulated ozone mixing ratios for the five trajectories on the two initial isentropic levels 650 K (top panel) and 600 K (bottom panel) corresponding to 74 and 97 ppb N_2O, respectively. The trajectories were chosen such that the considered air parcels stay close to the latitude indicated in the legend.

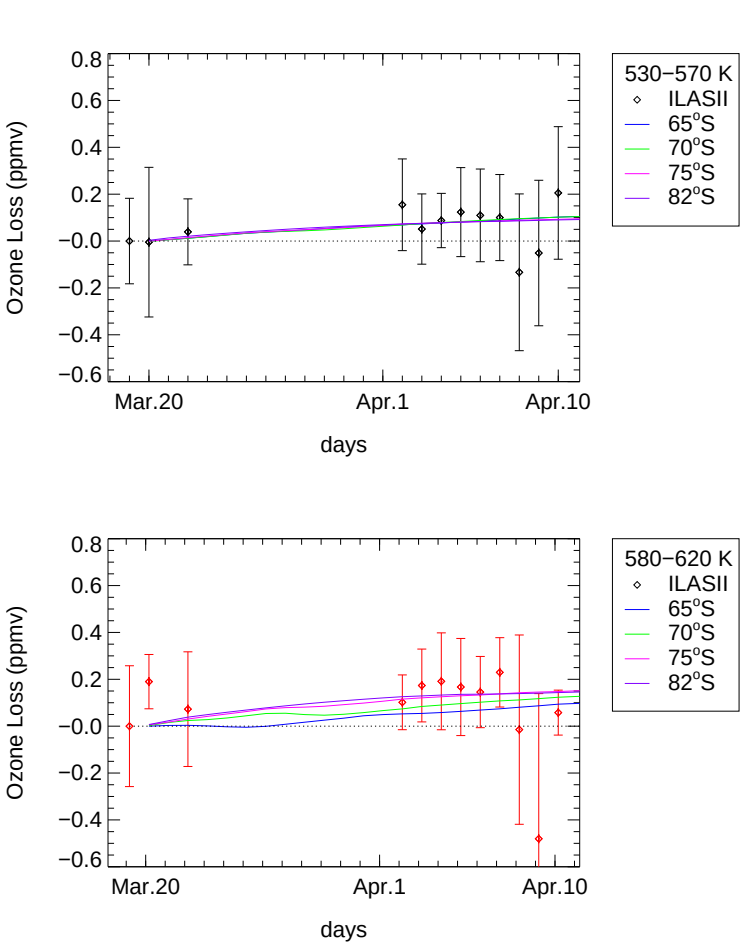

Figure 12. Colored diamonds: local accumulated ozone loss since March 20, 2003, derived using ILAS-II measurements, including the correction of results from different samples of air masses in March and April based on MIPAS observations, averaged for all profiles located within the polar vortex core [*Nash et al.*, 1996], with an accuracy of ozone mixing ratio less than 0.2 ppmv. Error bars describe the standard deviation of ozone loss for each day considered between March 19, and April 10, 2003. Colored lines: local accumulated ozone loss since March 20, 2003, derived using a CLaMS box model simulation for different equivalent altitude regions. Top panel: 74 ppbv N_2O level (580-620 K), bottom panel: 97 ppbv level (530-570 K).

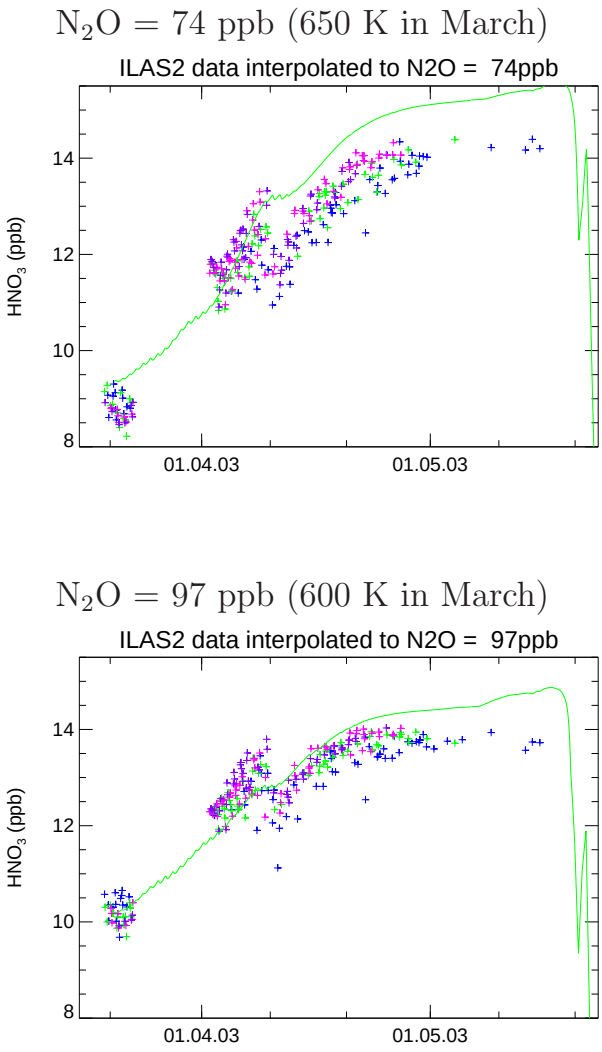

Figure 13. Colored plus signs: HNO_3 mixing ratios in different equivalent latitude regions, between March 19 and May 31, 2003, measured by the ILAS-II instrument. Green line: CLaMS box model simulations of HNO_3 initialized as described in the text at 82°S equivalent latitude.

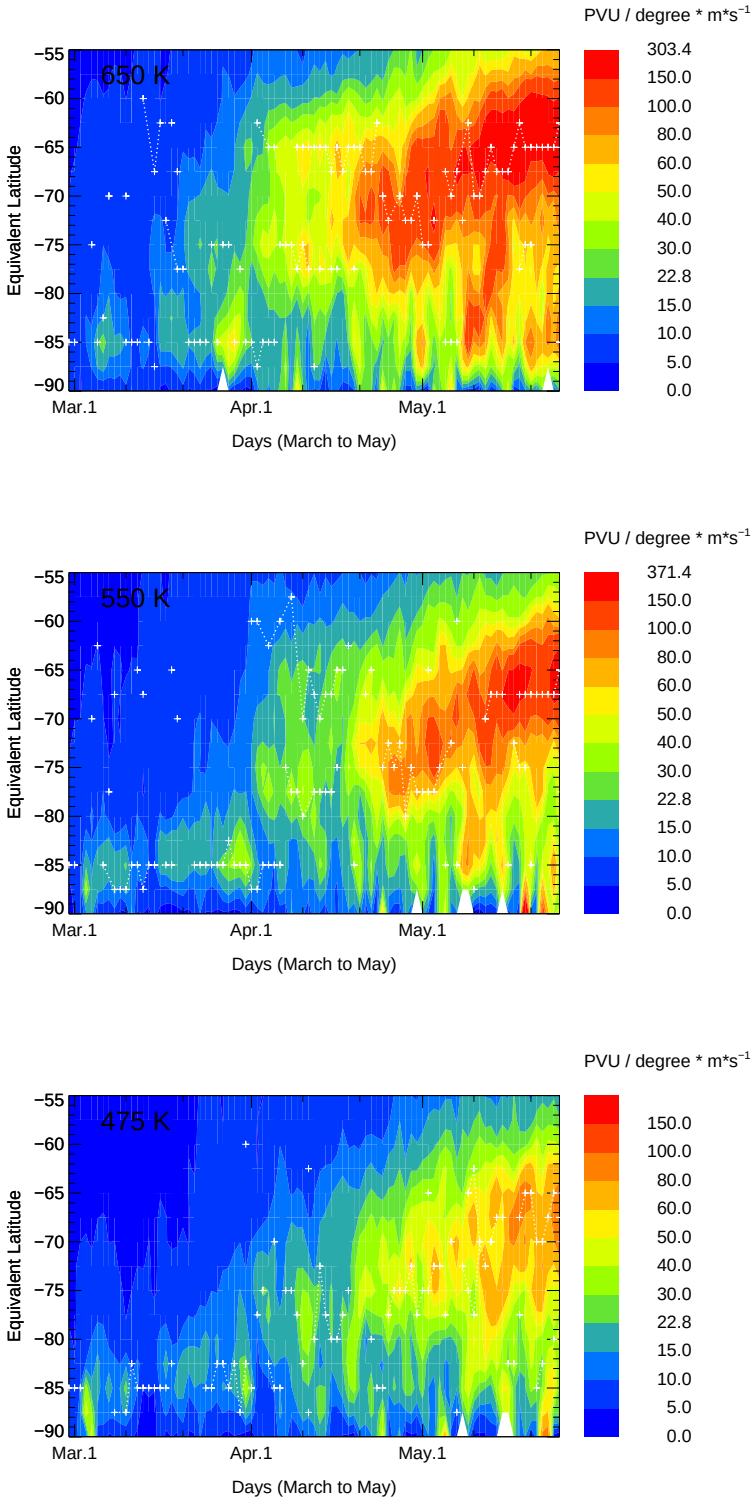

Figure 14. As Figure 1 but for 1997.

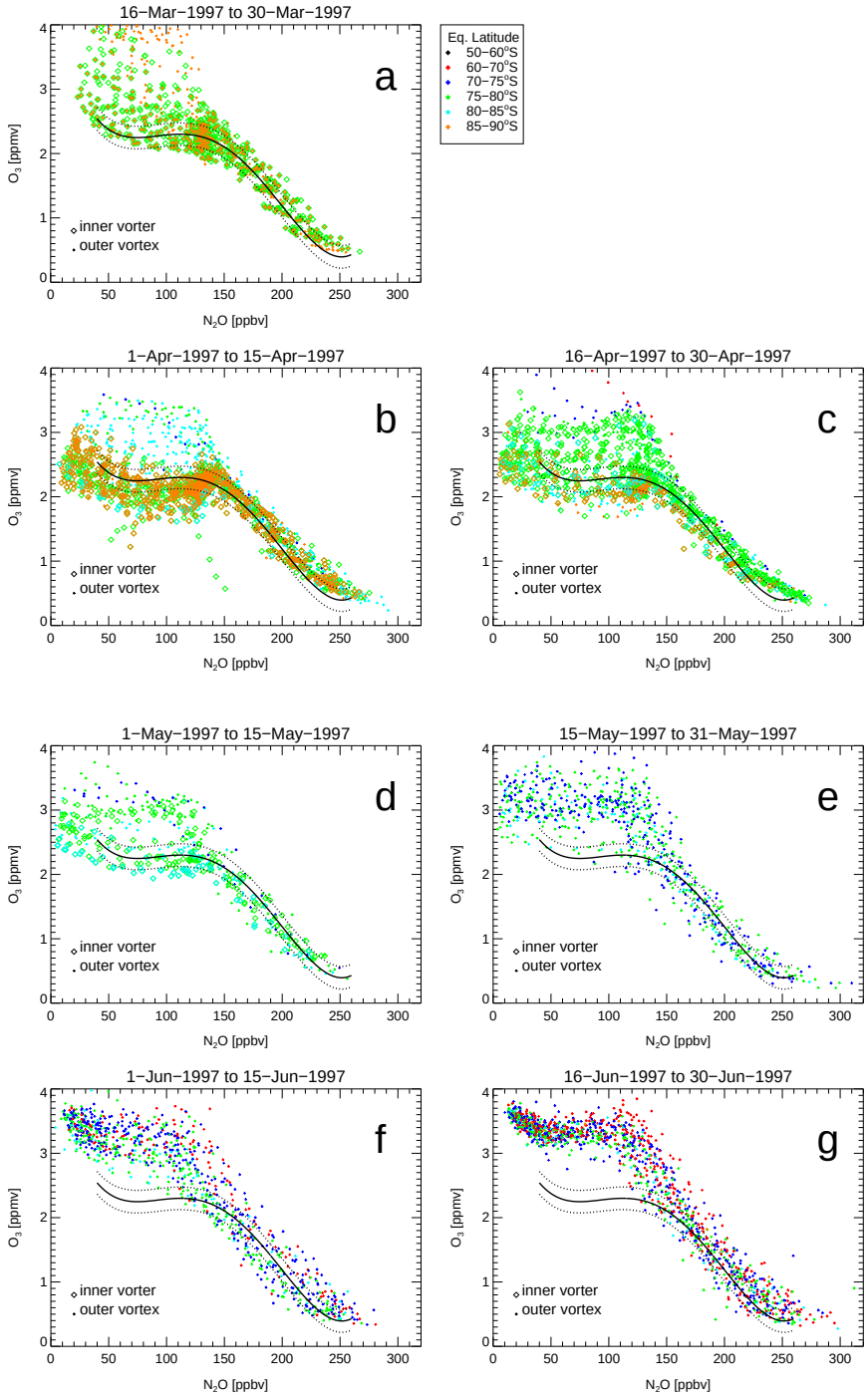

Figure 15. O_3/N_2O relation inside the early Antarctic vortex in 1997 prior to polar night from ILAS measurements for March 16-30 (panel a), April 1-15 (panel b), April 16-30 (panel c), May 1-15 (panel d), May 15-27 (panel e), June 1-15 (panel f), June 16-30 (panel g). Black line shown in each panel is a reference function derived as an empirical polynomial fit for March 16–30, 1997 (panel a) with the area of uncertainty derived from the standard deviation of the profiles (dotted lines). Different colors indicate different range of equivalent latitude of vortex profiles, see panel a and text.

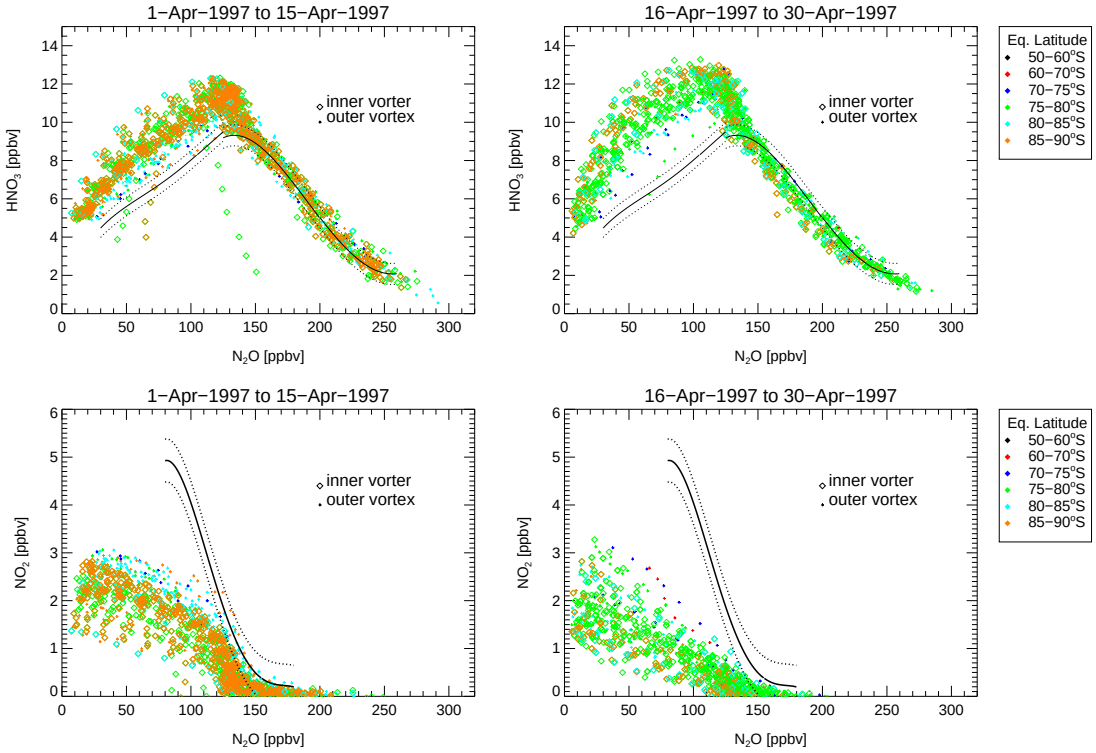

Figure 16. HNO_3/N_2O (top panel) and NO_2/N_2O (bottom panel) relation inside the early Antarctic vortex in 1997 prior to polar night from ILAS measurements for April 1-15 (left panel) and April 15-30 (middle panel). Black line shown in each panel is a reference function derived as an empirical polynomial fit for March 16–30, 1997 (not shown) with the area of uncertainty derived from the standard deviation of the profiles (dotted lines). Different colors indicate different range of equivalent latitude of vortex profiles, see right panel.

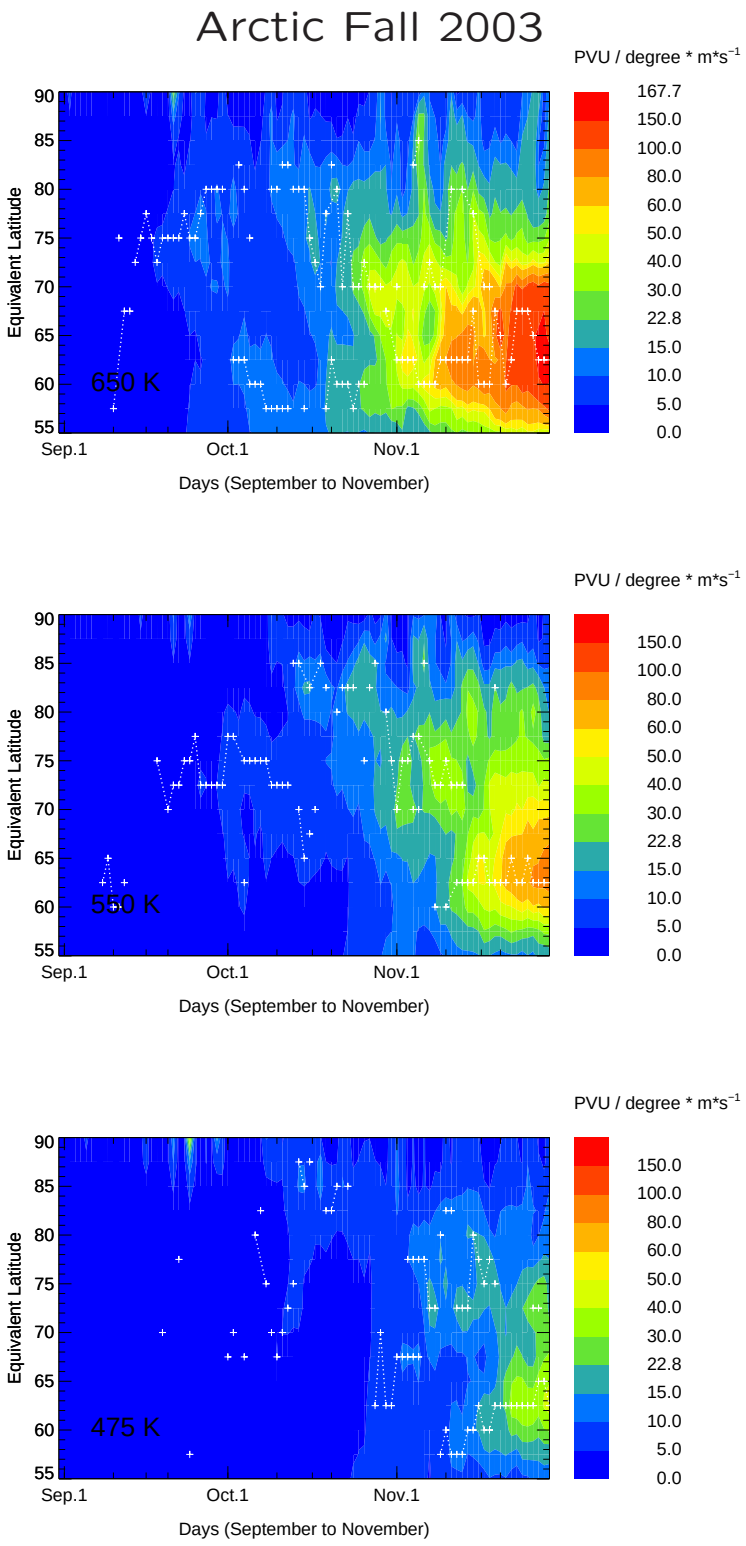

Figure 17. As Figure 1 but for the Arctic between September and November 2003.

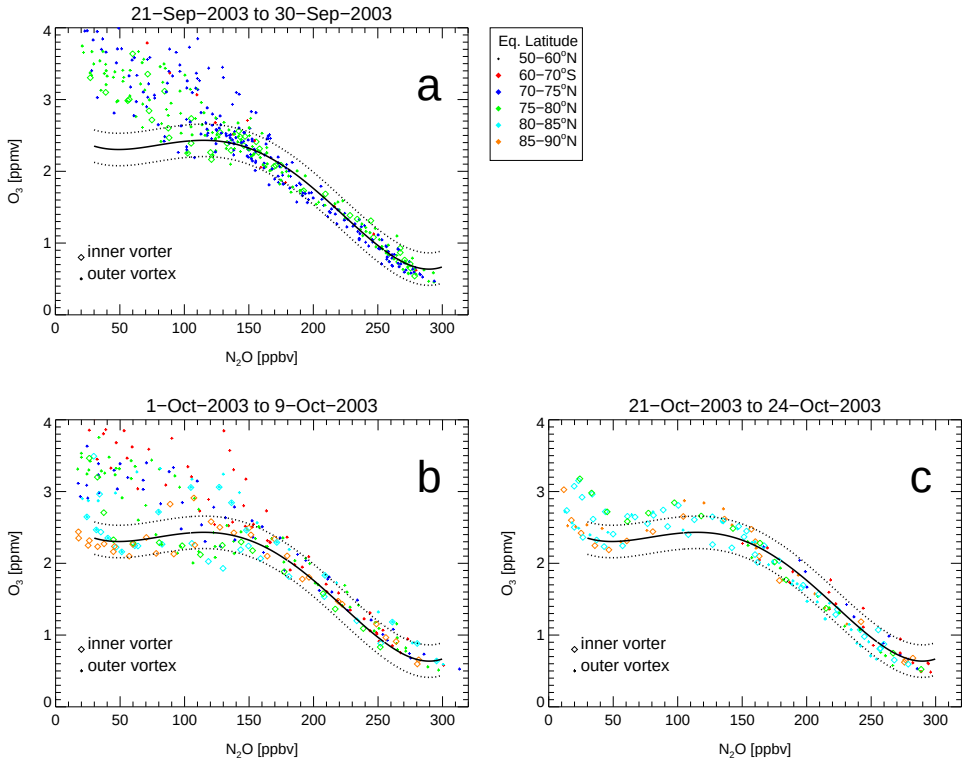

Figure 18. O_3/N_2O relation at high northern latitudes from ILAS-II measurements (panel a to c). Black line is the reference function derived in October 1-9 2003, for profiles observed poleward of 85°S equivalent latitude Different colors indicate different range of equivalent latitude of vortex profiles.

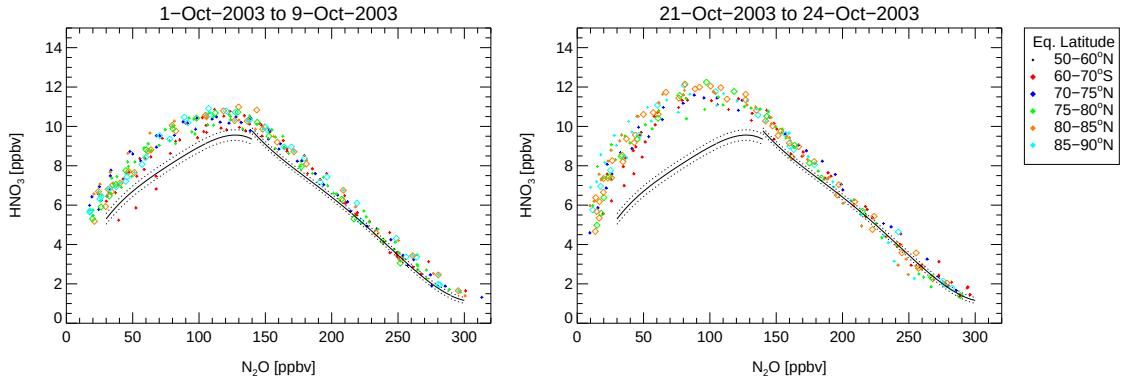

Figure 19. HNO_3/N_2O relations inside high northern latitudes from ILAS-II measurements in October 2003. Black line indicates the reference function derived from profiles measured at the end of September 2003 in high northern latitudes. Different colors indicate different range of equivalent latitude of vortex profiles.

Tables

Table 1. Sunlit hours per day at 550 K calculated from UK meteorological data within different equivalent latitudes

Year	Period	55-70°S(°N)	70-80°S(°N)	80-90°S(°N)
2003 Antarctic	March	13.0	13.6	13.1
1997 Antarctic	March	12.7	13.7	13.3
2003 Arctic	Sept.	13.4	14.3	14.9
2003 Antarctic	April 1-15	9.8	6.6	3.7
1997 Antarctic	April 1-15	9.7	6.5	4.5
2003 Arctic	Oct. 1-15	9.2	6.6	6.1
2003 Antarctic	April 16-30	8.5	4.2	0.4
1997 Antarctic	April 16-30	7.9	3.4	2.4
2003 Arctic	Oct. 16-30	6.8	4.6	4.2
2003 Antarctic	May 1-31	6.3	1.4	0.03
1997 Antarctic	May 1-31	6.3	1.2	0.1
2003 Arctic	Nov. 1-31	5.3	1.3	1.1